CYPRUS UNIVERSITY OF TECHNOLOGY

DEPARTMENT OF MECHANICAL ENGINEERING AND MATERIALS SCIENCE AND ENGINEERING

MASTER THESIS

EXPERIMENTAL INVESTIGATION OF THE EFFECTS OF RED BLOOD CELL AGGREGATION ON BLOOD FLOW

Theodorou Elena

Limassol 2016

CYPRUS UNIVERSITY OF TECHNOLOGY

DEPARTMENT OF MECHANICAL ENGINEERING AND MATERIALS SCIENCE AND ENGINEERING

MASTER THESIS

EXPERIMENTAL INVESTIGATION OF THE EFFECTS OF RED BLOOD CELL AGGREGATION ON BLOOD FLOW

Theodorou Elena

Academic Supervisor

Dr. Efstathios Kaliviotis

Limassol 2016

Copyright

The approval of the thesis by the Department of Mechanical Engineering and Materials Science and Engineering of Cyprus University of Technology does not necessarily implies acceptance of the views of the author from the Department.

In this section, I would like to express my feelings on behalf of those who gave me the strongest support to succeed. On the way for admitting this dissertation I have faced lots of difficulties and those people made me more powerful and gave me the proper positive energy to achieve my target.

I would like to give my warmest thanks, firstly, to my academic supervisor, Efstathios Kaliviotis. Within the last year I earned special knowledge from him and there is no doubt that this would definitely be a strong foundation from my future career.

Secondly, I would like to thank my family for the great support that they gave me while preparing the final work.

Finally, I want to thank my close friends, who always stood by me and contributed in their own way to the completion of my effort. Thank you.

In this personal place I would like to dedicate my thesis to my grandmother Thekla.

Grandmother this present thesis belongs to you. Thank you for everything...

ABSTRACT

Two-phase fluids consist of a dispersed phase suspended in a continuous medium with the former having the form of cells, particles, liquid droplets or gas bubbles. Understanding multiphase flows is important since they occur in many areas such as biological systems and industrial applications. Blood is a complex fluid which consists of various cells, proteins and other macromolecules. The main constituent of blood is the red blood cell (RBC) which accounts for approximately the 45% of the fluid at normal conditions and therefore blood can be approximated as a two phase fluid. The flow of blood at low shearing flow conditions is dominated by the effects of RBC aggregation (a reversible clustering of the cells) and other secondary effects such as network formation.

This project aims at studying blood flow in simple shearing flows and to analyze the changes in the flow characteristics (velocity, shear rate profiles, etc.) caused by the phenomenon of RBC aggregation. More specifically this project aims at studying specific parameters affecting the flow properties of blood, measuring the mean velocity of RBCs and how the velocity is affected by the phenomenon of aggregation and studying the various aggregation states, and how the shear forces affect the aggregation. Specialized software packages and particle tracking techniques will be used for the analysis of the flow with the prospect of modeling the observed flow behavior.

The main outcome of this present work is that the flow of blood at low shearing flow conditions is dominated by the effects of RBC aggregation and other secondary effects such as network formation. Analyzing the changes in the velocity profiles caused by the phenomenon of RBC aggregation and cell sedimentation can be support that the aggregation affects blood flow; in aggregative case of D70 and D2000 is observed medium for D70 and high aggregation for D2000 at low shear rates.

TABLE OF CONTENTS

Nomenclature

Abbreviations

RBC	**Red blood cell**
WBC	**White blood cell**
PIV	**Particle image velocimetry**
ESR	**Erythrocyte sedimentation rate**

Roman symbols

D	**Diameter**	**[µm]**
V	**Actual mean Velocity**	**[µm/s]**
Vmax	**Actual maximum Velocity**	**[µm/s]**
V*	**Normalized velocity [V/Vmax]**	
R	**Actual radius**	**[µm]**
rmax	**Actual maximum radius**	**[µm]**
r*	**Normalized radius[r/h]**	
h	**Actual gap of plates**	**[µm]**
n	**Viscosity**	**[mPas]**

Greek symbols

$\dot{\gamma}$	**Shear rate**	**[s^{-1}]**
τ_γ	**Yield stress**	
σ	**Shear stress**	

LIST OF TABLES

LIST OF PICTURES

Figure 37. D2000 gradient graphs a) D2000 gradient graphs, shear rate $5s^{-1}$ b) D2000 gradient graphs, shear rate $11s^{-1}$ c) D2000 gradient graphs, shear rate $25s^{-1}$ d) D2000 gradient graphs, shear rate 54

Figure 38. The aggregation volume of PBS, D70 and D2000

Figure 39.STDv Aggregation index for PBS,D70 and D2000

CHAPTER 1. INTRODUCTION

Blood is the fluid that circulates in the vascular system of humans; it transfers oxygen, nutrients and vitamins within the heart, tissue, arteries, veins and capillaries. Blood can be considered as a composite, two-phase fluid, due to the dominance of the red blood cell, which occupies a large proportion of the volume of the fluid. The comprehension of multiphase fluid flow is notably significant because such fluids are used in many areas, such as biological systems and industrial applications. Blood consists of various cells, proteins and macromolecules, which are held in the liquid phase (the plasma) and can be considered as a circulating tissue. Plasma consists of 92% of water and 8% of protein solution. As mentioned, the main blood component is the Red Blood Cell (RBC), which occupies approximately the 45% of the fluid, under standard conditions for the male and 40% for the female population. Blood is a non-Newtonian fluid, and its mechanical properties depend on hematocrit, which is the volume percentage of red blood cells in blood, the phenomenon of red blood cell aggregation, and the deformability of the RBC.

The blood flow under low shear stresses favors red blood cell aggregation and aggregate network formation [1]. Under low shear stresses the aggregate size increases and the stress which develops on aggregating erythrocytes influence the viscosity of the fluid. The aggregates are proportional to the magnitude of shear forces [2]. Viscosity is the resistance which develops while the blood is flowing and depends on shear stresses. Parameters that influence the viscosity of blood include the hematocrit, plasma viscosity, RBC aggregation and the mechanical properties of the highly deformable RBCs [3]. Blood viscosity decreases as the shear forces get larger.

Rheology can be described as the study of flow and deformation of matter. Hemorheology is the study of flow and deformation of the formed elements of blood mainly the RBC. Figure 1 presents graphically the movement of erythrocytes in the human body vessel carrying oxygen to the body tissue. The flow behavior of RBC (Figure 1) and its tendency to aggregate plays an important role in many pathological phenomena such as coagulation, hypertension, diabetes mellitus, sepsis, cardiovascular diseases and hematological diseases. In this thesis the influence of RBC aggregation on blood flow is investigated for blood flowing in a simple shear device. Various shear conditions are developed and the intensity of the aggregation

phenomenon is altered in order to examine aggregation effects in the flow characteristics.

Simple shear flows are used extensively in rheometry for the measurement of shearing stress and the calculation of various fluid properties (viscosity, viscoelasticity, RBC aggregation) due to the uniform shearing conditions they offer. In the present work the geometry was chosen so that a convenient shearing flow field for visualization and analysis of the phenomenon of RBC aggregation was produced and used.

Figure 1. Pictorial representation of the movement of erythrocytes in a human body vessel (1)

In this first chapter of the thesis a review of previous work on blood flow and RBC aggregation is given. In the beginning essential background information is provided, followed by information on aggregation and blood flow. A third section describes the techniques for measuring the mechanical and flow properties of blood. A final section provides a summary and the rationale of the project.

1.1Historical perspectives

The need of people to understand diseases and to develop a medical theory initially led on the concept of "humors". This concept was a direct application of Greek natural philosophy developed by Hippocrates the father of humoral pathology. This medical theory declares that the human body contains a well-balanced mixture of four juices, the sanguine, the melancholic, the phlegmatic and the choleric. Disease could be caused if the balance of these juices is not stable. The way that the physicians diagnosed the diseases was the behavior of blood, taking some blood samples from the patients. The melancholic humor was the lowest dark part of blood, the choleric humor was the serum separating from clotting blood and the sanguine was representing by RBC.

For better understanding of blood flow behavior Herman Boerhaave on 17th century , enrich the medical ideas using intravital microscopy, a tool that enables imaging subcellular structures in several biological processes in live animals. In the mid of 19th century, Poiseuille made significant contribution to physiology and fluid mechanics by observing the flow behavior of fluids in glass capillary tubes and developing the well-known Poiseuille's law for tube flow.

$$\Delta P = \frac{8\mu LQ}{\pi r^4} \quad (1)$$

ΔP=Pressure loss

L=length of pipe

μ=dynamic viscosity

Q= volumetric flow rate

r=radius

At the end of 19th century Rudolf Virchow introduced a new concept of disease which was correlated with the structural and functional disturbances of cells, which can be diagnosed by microscope.

At the beginning of the 20th century, Robin Fahraeus correlate the idea of humoral juices with a modern idea, suggesting that the suspension stability and the fluidity of blood changed during disease [4].

1.2 Blood characteristics

An average adult has 4.7 to 5.6 liters of blood which is made up of plasma, RBCs, WBCs and platelets. The red color of RBCs is due to the cytoplasm of erythrocytes, which is rich in hemoglobin, an iron-containing biomolecule which binds oxygen.

The red-cell membrane is a lipid bilayer covered by a glycocalyx and it is based on the cytoskeleton [5]. The cytoskeleton is a network of intercollated proteins. The membrane flexibility, integrity and deformability depend on the mechanical properties of the cell membrane. The human body produces approximately 2.4 million new erythrocytes per second [6, 7]. The size of RBCs is 8 micrometers in diameter approximately, but varies due to pathologies. Each human red blood cell is about 2μm thick and contains approximately 30pg of hemoglobin (generally 900g in the

circulating human system).White blood cells (WBCs) are the cells of the immune system, which are responsible for the protection of the body by attacking viruses, bacteria and germs. WBCs are also called leukocytes and their size is approximately 10 micrometers in diameter and platelets are 3μm in diameter.

As it was mentioned previously, viscosity is the resistance which develops while the blood is flowing and depends on shear stress. Blood viscosity can be considered as an index of the thickness and stickiness of blood [8]. As mentioned earlier, the main parameters that influence the viscosity of blood is the hematocrit, plasma viscosity, RBC aggregation and the mechanical properties of RBCs [9]. In Table 1 is presented the plasma viscosity of normal subjects in different temperatures. Plasma viscosity of a normal adult is approximately 1.25 mPas at 37°C[10]. Plasma is a Newtonian fluid and its main component is fibrinogen which is the major protein in terms of concentration. Plasma viscosity depends on the molecular weight and structure of plasma proteins. The presence of large molecular weight and the shape of proteins increases plasma viscosity. In addition if we increase the viscosity, we decrease the sedimentation rate of erythrocyte (ESR). Plasma fibrinogen is a soluble glycoprotein and is associated with cardiovascular diseases. Scientists in previous studies, refer that the increased fibrinogen concentrations indicate presence of inflammation. Generally increase in blood viscosity, increases thrombus formation and aggregation [8].

			Plasma viscosity (mPaS)		
Temperature °C	Sex	Number of tests	Range	Mean	Standard deviation
20	—	—	1.70-1.915	—	—
25[a]	Male	96	1.50-1.72	1.64	0.049
	Female	63	1.50-1.72	1.63	0.056
	Combined	159	1.50-1.72	1.64	0.052
37	—	—	1.16-1.35	—	—

Table 1. Plasma viscosity values in normal subjects [10]

1.3 The circulatory system

The circulatory system is the blood transport system, which is connected with body cells and tissue. The system permits blood to circulate and is responsible for

supplying oxygen and substances to the tissues. It carries away the carbon dioxide to the lugs. The blood is pumped through a closed system of blood vessels by the heart. The circulatory system also called cardiovascular consists of the heart (cardiovascular), lungs (pulmonary) arteries, veins and vessels (systemic). Approximately 7500 liters of blood travels daily through 97000Km of blood vessels.

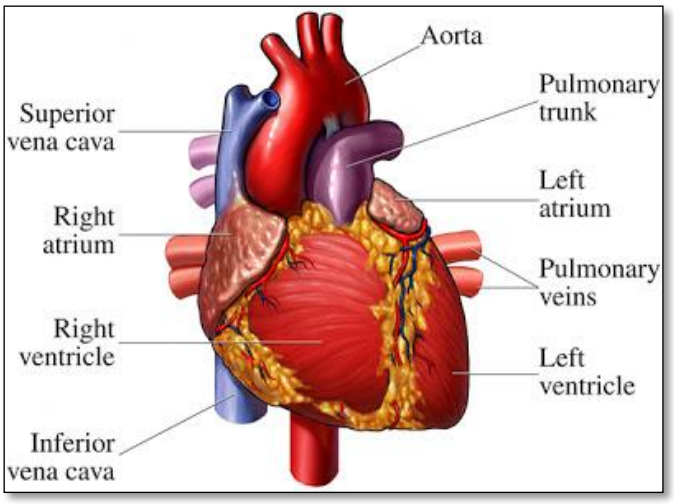

Figure 2.Anatomy of the human heart [2]

Heart is a muscular organ and consists of four chambers: left atrium, right atrium, left ventricle and right ventricle. The right atrium receives blood for the veins and pumps it to the right ventricle. The right ventricle receives blood from the right atrium and pumps it to the lungs where it is loaded with oxygen. The oxygenated blood is received by left atrium from the lungs and pumps it to the left ventricle. From the left ventricle blood is pumped through the arteries and arterioles to the capillaries, where it equilibrates with the interstitial fluid. Finally the strongest chamber (left ventricle) pumps oxygen to the rest of body.

The pulmonary circulatory system sends oxygen-depleted blood away from the heart through the pulmonary artery to the lugs and returns oxygenated blood to the heart through the pulmonary vein. When blood gets in to the lungs, carbon dioxide is released from the blood and oxygen is absorbed. The pulmonary vein directs the oxygen rich blood back to the left atrium of the heart [11].

1.4 Pathologies related to blood flow

The flow behavior of RBC plays an important role in many pathological phenomena such as the phenomenon of coagulation, hypertension, diabetes mellitus, sepsis,

cardiovascular diseases and hematological diseases. Hematocrit is the volume percentage of red blood cells and its value may cause disease. Under pathological diseases the Hematocrit value is high due to increment of viscosity. Blood diseases can be diagnosed by measuring the hematocrit levels in the blood.

Diabetes is a disease which is accompanied by metabolic disturbances, in which there are high blood sugar levels in the blood. Increasing the levels of sugar in our blood we increase the changes developing diabetes. In disease of Diabetes, plasma and blood viscosity are increased which enhanced RBC aggregation and altered RBC deformability [12].

Sepsis is a complex syndrome. In most patients the sepsis syndrome starts with infection in the lungs. Sepsis is the most dangerous disease in the elderly and the diagnosis is more effective when is performed at the first stages of the disease. Figure 3 illustrates blood infected with sepsis bacteria.

Figure 3. Staph bacterial sepsis infection image with scanning electron

Cardiovascular disease is the disease of the heart and blood vessels. Heart attack, ischemic diseases, heart valve problems, arrhythmia are the main diseases of cardiovascular system [13]. The increased viscosity and aggregation is significantly associated with the development of cardiovascular diseases.

Hypertension is a chronic pathohphysiological disease, which is related with high blood flow pressure. Hypertension is the common cause of vascular damage and it is diagnosed by the two measurements of blood pressure, the systolic and the diastolic pressure. The systolic is the minimum pressure and the diastolic is the maximum pressure. Increase in the viscosity of blood is associated with the high blood pressure. According to the following figures, figure 5 shows the schematic differences between normal and anemic amount of RBCs and figure 4 shows the effect of plaque formation in blood vessel.

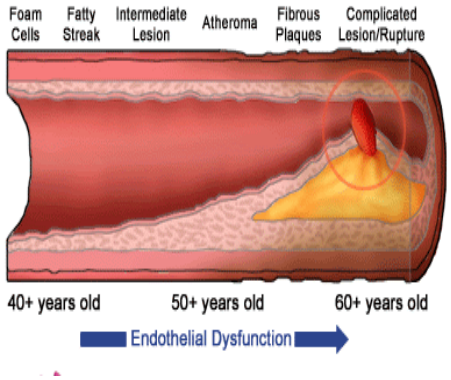

Figure 4. Representative illustration of the mechanism that Hypertension damages the blood vessel

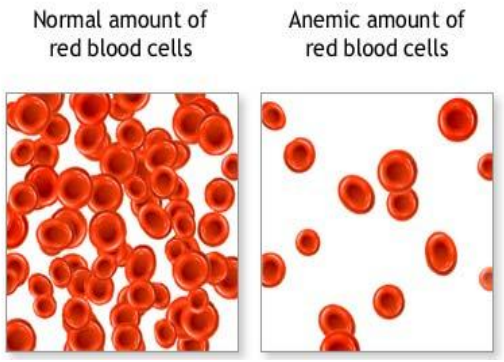

Figure 5. A picture of a normal and anemic amount red blood cells

1.5 Blood rheology and hemodynamics

Rheology is the field related with the study of the flow and deformation behavior of materials under applied forces. Deformation refers to any changes in the shape or size of an object due to applied force or a change of temperature [11].

If we apply a force on an elastic material, and the deformation is not large, the original shape of the material will return when the force is subtracted. The reversible behavior often shows a linear relation between stress and strain. In the case that the deformation of the material is not reversible, the material is determined as plastic material and the non-reversible behavior shows non-linear relation between stress and strain. In a Newtonian fluid the behavior shows linear relation between stress and rate of shearing strain.

Non-Newtonian fluids are the fluids in which the dependence of the shear stress to shear rate is not linear. Figure 6 shows the behavior of the shear stress under shear rate and the influence on shear thinning and shear thickening. The viscosity of a shear thickening fluids seems to increase when the shear stress increases. On the other hand in shear thinning fluids, or pseudo plastic fluid, its viscosity decreases with increasing shear stress. Bingham plastic fluids are the fluids which have linear relationship between shear stress and shear strain but its line do not pass from the origin. In order to begin to flow they need a finite yield stress.

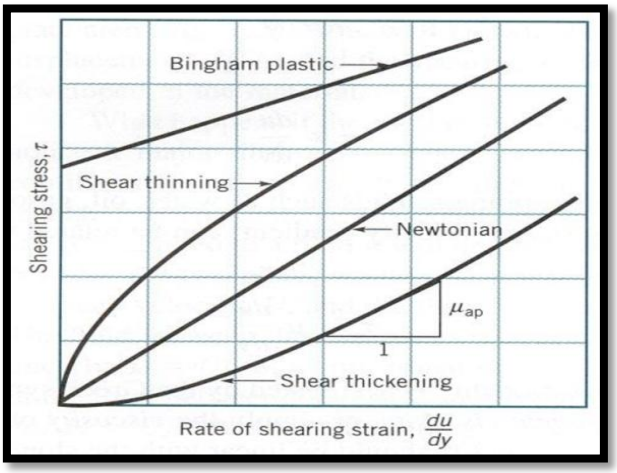

Figure 6. The response of shear stress for different fluids under shear rate (rate of shearing strain) and the shear thinning and shear thickening behavior.

Below the various responses of shear stress as a function of the shear rate are listed in more detail:

Shear-thinning: The viscosity decreases with shear rate due to the flow, the internal structure brakes.

Shear thickening: The viscosity increases with the shear rate, due to the microstructure disturbance of the fluids.

Certain fluids do not flow if the pressure is below a critical value. Such fluids are weak gels, toothpaste and ketchup; this property is called yield stress.

Many fluids show viscoelastic behavior. Viscoelasticity is the property of materials which exhibit viscous and elastic behavior when a stress is applied. Stress is the deforming force, applied per unit area. There are two types of stresses: shear stresses, which are acting parallel to the surface, and normal stresses, which are acting

perpendicular to the surface. The degree of deformation is the strain and the rate of deformation is the shearing strain rate or shear rate.

In terms of rheometric flows the laminar flow is the relevant state of flow, where rheological measurements take place. Laminar is the flow which is strongly affected by the viscous forces, and in which fluid particles move along smooth trajectories. Under laminar flow, shear forces are used to determine fluid flow. The internal resistance which the flow adduces is the viscosity of the fluid. Turbulence flow is the flow which is characterized by eddies and recirculation and is controlled by powerful forces by which the fluid particles move irregularly among turbulent trajectories [14].

Some Newtonian fluids are independent of shear stresses and rate, but still exhibits normal stress-differences and in non-Newtonian fluids the viscosity depends on shear rate.

Results such as those presented in Figure 6 are usually obtained from utilizing simple shear flows, which can be produced by geometries approximating the parallel plate flow (Figure 7). In a steady shear flow for a fluid confined between two parallel plates, with one of them moving at a constant velocity V (as described in Figure 7) the velocity can be described by:

$$u = \dot{\gamma} y, \quad v_y = v_z = 0 \quad (1)$$

The shear stress is:

$$\sigma_{xy} = \sigma = \dot{\gamma}\eta(\dot{\gamma}) \quad (2) \qquad \sigma_{xz} = \sigma_{yz} = 0 \quad (3)$$

$$\sigma_{xx} - \sigma_{yy} = N_1(\dot{\gamma}) = \Psi_1 \dot{\gamma}^2 \quad (4)$$

$$\sigma_{yy} - \sigma_{zz} = N_2(\dot{\gamma}) = \Psi_2 \dot{\gamma}^2 \quad (5)$$

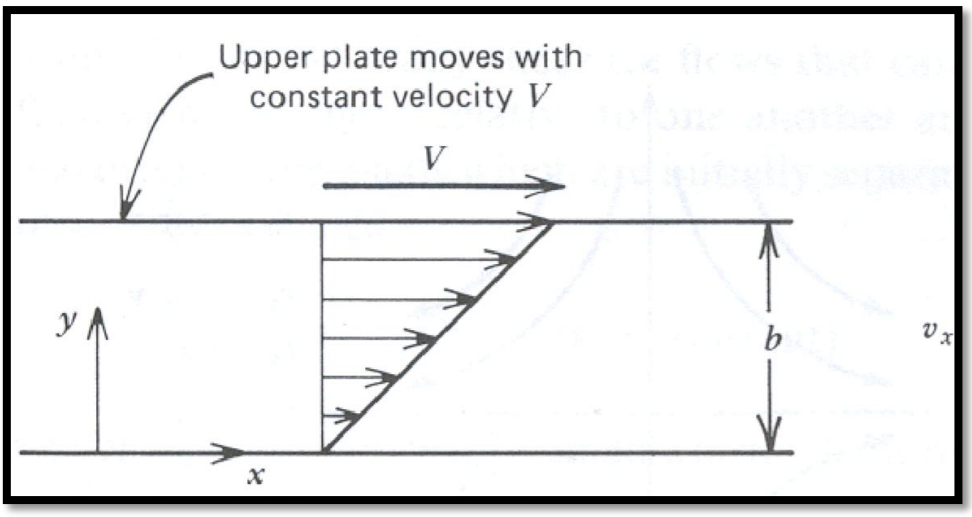

Figure 7.The velocity profile of an upper plate which moves with constant velocity V

where η is the viscosity of the fluid, N_1 is the first normal stress difference the Ψ_1, Ψ_2 is the factor, and N_2 is the second normal stress difference.

1.5.1 Factors affecting the rheological properties of blood and aggregation

The membrane of the RBC is a network of proteins and is mainly responsible for the maintenance of biconcave-discoid shape. Also the RBC exhibits viscoelastic behavior. RBCs mechanical properties depend on the force which we apply to them. If we apply a discrete force on them we react on their mechanical properties changing their shape and thickness.

The blood flow under low shear stresses favors the red blood cell aggregation and the network formation [1]. Under low shear stresses the size of aggregates increases.

The most important protein that influence the phenomenon of aggregation is the fibrinogen. Fibrinogen is a glycoprotein, a blood plasma protein . The increase or reduction of fibrinogen concentrations, results in enhanced RBCs aggregation. Low levels of fibrinogen can cause thrombosis due to coagulation activity and this can lead to serious medical conditions such as heart attack, sepsis and stroke and higher levels causes inflammation. Fibrinogen level increases in pregnancy.

1.5.2 Non-Newtonian characteristics of blood viscosity

Blood as a non-Newtonian fluid does not follow the linear relationship between stress and shear rate. For this reason other viscosity and stress models have been developed. The most widely acceptable models are described below.

1.5.2.1 Power Law Model

$$\sigma = k|\dot{\gamma}|^n$$

$$n < 1\,, pseudoplastic\ or\ shear\ thinning$$

$$\dot{\gamma} = \text{shear rate}$$

$$\text{n} = \text{viscosity}$$

Pseudoplastic fluids are the fluids which are usually solution of polymeric molecules and have lower apparent viscosity at higher shear rates thus as we increase shear rate we get lower resistance. The power law model has been used extensively in the literature to describe blood viscosity [15].

$$n = 1, k = n\,, Newtonian\ fluids$$

$$n > 1, Shear\ thickening$$

Where n is the line gradient and the $\log(\text{n}) / \log(\dot{\gamma})$ correlates with the magnitude of fluid viscosity. The value of $\log(\text{K})$ is the point where the line intersects the n axis.

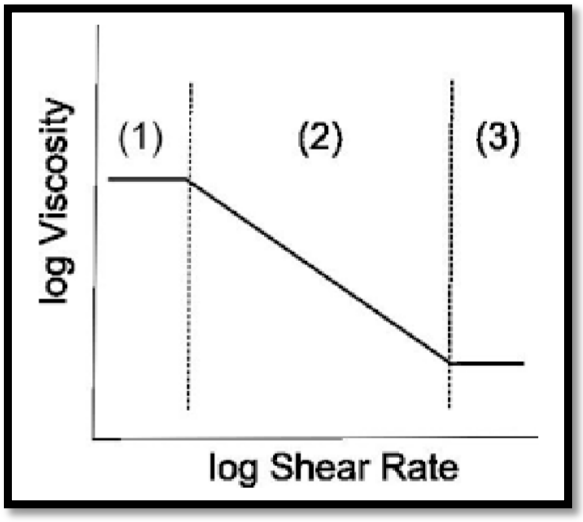

Figure 8.Viscosity against shear rate

1.5.2.2 Careau-Yasuda Model

Carreau-Yasuda is a blood viscosity model of non-Newtonian fluid which has been used to describe the non-linear dependency also. It has been also used to compare two-dimensional Newtonian and non-Newtonian flows in pipe geometries [16] Carreau Yasuda flows exhibits significant differences in the steady state flow situation compared to the power law behavior. At curved pipe the model exposes significant differences in magnitude and shear rate. From previous studies it

mentioned that in curved pipe in the centre of geometry we observe differences in velocity and near walls of geometry we observe larger differences in shear rate.[17,18,19]. The following equation illustrates the Careau-Yasuda model.

$$\frac{\mathrm{n}(\dot{\gamma}) - n_{\infty}}{(\mathrm{n_o} - \mathrm{n}_{\infty})} = \left[1 + (\dot{\gamma\lambda})^{\mathrm{n}}\right]^{(\mathrm{n}-1/\alpha)}$$

n_{∞}=high shear rate viscosity

n_{o}= low shear rate viscosity

α =the exponent which defines the metabatic behavior from low shear viscosity to high shear viscosity

λ= Time constant which defines the metabatic shear rate

$\dot{\gamma} =$ shear rate

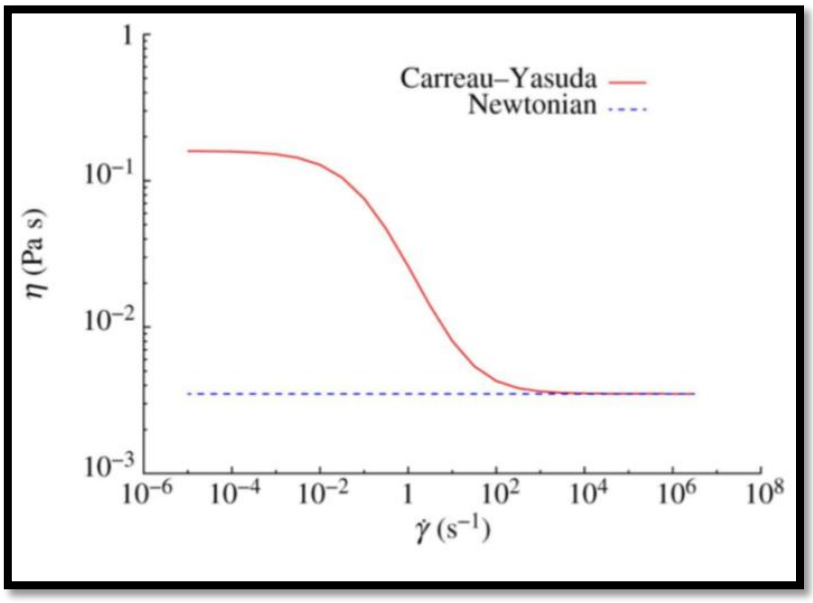

Figure 9.Carreau-Yasuda model

1.5.2.3. Bingham Model

Bingham Model is the model which shows the behavior of plastic liquid compared with Newtonian (viscous) fluid in many geometries. Picture 10 shows the behavior of Newtonian fluid in red color and the behavior of Bingham plastic liquid in blue color. In horizontal axis is shear rate and in vertical axis is shear stress. The fluid can be only flow if the pressure at the end of a pipe is increased. This increase produce stress on the fluid which incline it to move. Bingham plastic fluids can flow only if the stress outreach a specific value, the yield stress. For the Newtonian fluid the slope of

graph is viscosity and for the Bingham plastic in order to describe the viscosity we need two parameters: the yield stress and the slope.

$$\mathrm{n}(\dot{\gamma}) = \infty, \gamma\iota\alpha\ \tau \leq \tau_y$$

$$\mathrm{n}(\dot{\gamma}) = \mathrm{n}_\infty + \tau_\mathrm{y}/\dot{\gamma}$$

$$n_\infty = high\ shear\ viscosity$$

$$\tau_y = yield\ stress$$

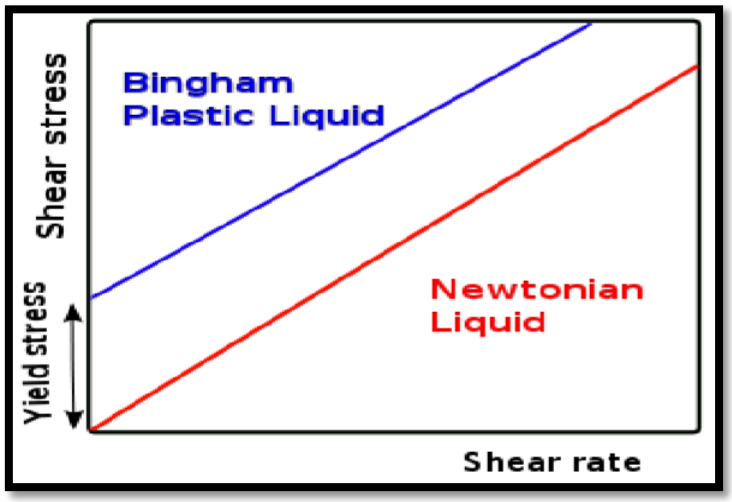

Figure 10. Bingham Model

1.6 Techniques to measure blood velocity

In the analysis of blood flow behavior it is important to characterize the flow of red blood cells in various simple and complex geometries. For this reason various techniques have been developed, with particle image velocimetry (PIV) being the most popular one. Particle image velocimetry is an optical method of flow visualization used to obtain instantaneous velocity measurements and related properties in fluids [17,18,19]. Standard PIV techniques measures two velocity components in a plane using camera and a laser light source system.

MicroPIV is an optical method used in micro fluidics. With the use of an epifluorescent microscope velocity of particles can be measured in micro channels, vessels and flow devices .The fluorescing particles which are exanimate are in specific wavelength and emit at another wavelength. MicroPIV uses a laser light which is reflected through a mirror and travels through an objective lens that focuses on the point which is under observation. The emission from the fluorescing particles, along with reflected laser light, shines back through the objective, the mirror and

through an emission filter that blocks the laser light. The motion of the seeding particles is used to calculate speed and direction of the flow being studied. In that way microPIV method focus only ον one plane at a time, but it creates two dimensional planes[20][21].

Figure 11 shows the vector fields of a surface-tension driven Hele-Shaw flow around a 30μm wide obstacle. Each field contains approximately 900 velocity vectors covering a 120μm x 120μm field of view. Each velocity vector was measured with a 6.9μm x 6.9μm x 1.5μm measurement volume. It shows the instantaneous vector field measurement and picture b shows the eight-image ensemble-averaged PIV velocity vector field.

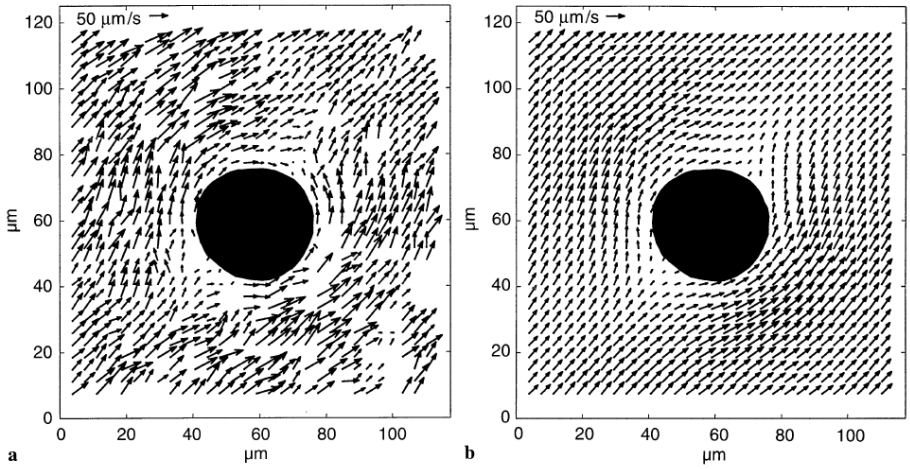

Figure 11. Vector fields of a surface-tension driven Hele-Shaw flow around a 30μm wide obstacle

The technique used to measure blood velocity in the present work is JPIV. The JPIV software program is a particular program which calculates the velocity of particles in various flows and can be applied in micro scale flows also. JPIV correlates the motion of a large number of cells and calculates the averaged cell velocity. This method estimates the movement of big number of red blood cells based on pattern correlation techniques. This method may have advantages compared to other techniques because a wide spectrum of RBCs, and no individual cells, is analyzed [3]. A more detailed description of the JPIV program is provided in the Methodology section.

Studies using the JPIV method include this of Bitsch et al.,2005; Lima et al. , 2006, 2007 , 2008, Sugi et al.,2002; Hove et al.,2003; Vennemann et al.,2006; and Lee et al.,2007) in micro-PIV has been applied in vitro blood flows within simple channels, as well as to in vivo flows in rats, zebrafish , embryos and chicken embryos. In those

studies it was shown that at higher shear rates the red blood cells tends to disaggregate. Intensity gradients of images is the aforementioned change in the images properties. The intensity gradients due to the aggregation forces tends to change with the change of shear rates. The decrease of shear rate, causes the phenomenon of aggregation. JPIV technique investigated that the effect of Hematocrit play an important role in technique accuracy. The aggregation factor affect the accuracy of technique.

Velocity fields from figure 12 were analyzed using an optical shearing microscope and PIV. Blood at 45% haematocrit was sheared at rates of $5.4 < \gamma < 25.2\ s^{-1}$ and imaged using a high speed camera. The geometry consisted of two glass plates ,the lower plate was driven by a stepper motor to shear the blood in z direction with a nominal shear rate γ that was controlled by the lower plate., changing the rotational velocity ω. The plates were separated with gap of 30μm, Figure 12 shows the velocity profile of $\left[\frac{V}{V_o}\right]$ accross $\frac{\mathrm{x}}{\mathrm{R}} = 1$ for different shear rates and the comparison between them. The $\left[\frac{V}{V_o}\right]$ determines the velocity magnitudes which is normalized by the Vo. The dotted line represents the expected changes of the velocity for a Newtonian fluid. The behavior at γ=54.4, 25.2 and 11.7s^{-1} is closer to the Newtonian behavior due to the dispersion of aggregates. The solid body rotation like behavior seen in γ=5. 4s^{-1} is associated with the formation of strong network[3].

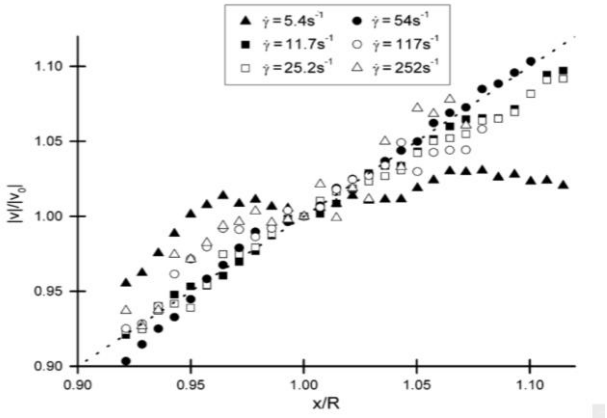

Figure 12 .Radial velocity profile of $\left[\frac{V}{V_o}\right]$ across $\frac{\mathrm{x}}{\mathrm{R}} = 1$ for different shear rates and the comparison between them[3]

1.7 Techniques to measure RBC aggregation

In the literature there are plenty techniques to analyze and measure RBC aggregation including ESR rate test, Microscopic and optical techniques and Ultrasonic back-scattering technique [22].

Sowemimo-Coker and co-workers [23] measured the red blood cell aggregation phenomenon from various healthy human samples of blood using the following methodology: they placed the blood samples in autologous plasma or, after washing the cells free of plasma proteins, in phosphate buffered saline containing 3% dextran 70 (MW = 73 kDa); all suspensions were made to the same haematocrit of 40%, and the degree of cellular aggregation was measured using the Myrenne Erythrocyte Aggregometer that is based on a light transmission technique[24]. The Myrenne erythrocyte aggregometer is an optical method to measure the aggregation phenomenon and has certain limitations in its accuracy [25]. It gives a wide range of values both in healthy and disease. making results less comparable due to the fact it gives two aggregation indexes depending on the rotation speed of the cone MO(at stasis) and M1(at $3s^{-1}$) and time elapsed (5 or 10 sec), after the cone is topped abruptly

Optical methods use a laser light source and light detection sensors to measure the amount of light transmitted or back-scattered when a thin layer of blood is illuminated. The changes of light transmission can be analyzed for various shear rates produced in different geometries.

Hitt and Lowe [26] used Fourier methods and computer simulator to measure the cell aggregation. They examine the spatial patterns of transmitted light intensities of in vitro aggregating blood flow. Although the analysis was capable only of providing approximate bounds for the aggregate sizes due to the broadness of the Fourier spectrum.

In another study of Kaliviotis et al (2010) the technique which was used to measure RBCs aggregation was based on intensity gradients; the aforementioned changes in properties in the images properties which change with the shear rate. The samples were subjected under different shear stresses at the range of $5.4 \leq \gamma \leq 2\dot{5}.2s^{-1}$; In this study it was observed that blood viscosity increases 2 orders of magnitude as the shear rate decreases. As we increase the shear forces the aggregates broken down to individual cells. In addition it was observed that the aggregation of cells depends not

only on the hematocrit, the properties of plasma and RBC, but on the geometry of the experimental system also.

1.8 Summary and purpose of thesis

This project aims at studying blood flow in simple shearing flows and to analyze the changes in the flow characteristics (velocity, shear rate profiles, etc.) caused by the phenomenon of RBC aggregation. More specifically this project aims at:

- studying specific parameters affecting the flow properties of blood.
- measuring the mean velocity of RBCs and how the velocity is affected by the phenomenon of aggregation.
- studying the various aggregation states, and how the shear forces affect the aggregation.
- assessing the possibility of using a novel flow configuration for the study of the properties of aggregating 2-phase fluids.

The importance of performing this study is due to the reason that the phenomenon of RBCs aggregation is present in pathological conditions. The flow behavior of RBC plays an important role in many pathological phenomena such as the phenomenon of coagulation, hypertension, diabetes mellitus, Sepsis, cardiovascular diseases and hematological diseases. Also high blood viscosity is associated with mortality.

In addition, recently there is a great interest from the scientific community to develop micro fluidic applications for use in novel diagnostic systems. Those diagnostic system operate in the micro scale and therefore understanding of flow of blood in that scale is very important. However, blood flow behavior in the micro scale has not studied in detailed so far. For example microPIV studies including aggregating samples are rare in the literature. The present work would also contribute in this direction too.

CHAPTER 2. METHODOLOGY

In this chapter a detailed description of the techniques, methods and experimental apparatuses used to perform the study will be described.

2.1 The blood samples

The blood samples were collected in bottles of 10ml preloaded with 1.2 anticoagulant agent EDTA. The Hematocrit of all the samples was determined by centrifugation at 3000rpm for 10min and adjusted to 45% (packed cell volume). Test was completed within 4h of sample collection. The study was approved by the Research Ethics Committee (South East London REC, CREC ref. 04/05-15). The samples were treated to create two different states of aggregation intensity; no aggregation and moderate aggregation. For the no-aggregation state RBCs were suspended in phosphate buffer saline (PBS). For the aggregation case the samples were suspended in PBS solutions containing Dextran of two different molecular weights (70000, and 2000000 mw). Dextran is a type of polysaccharide that is widely used to induce aggregation in blood samples. For every aggregation state similar shear rates were used that affected the blood flow.

2.2 Camera and PIV software

The JPIV program is a particular program for measuring the displacement of particle pattern. In contrast to many other techniques, that measure the velocity of a single point JPIV calculates the 2D velocity fields(two Cartesian velocity components),parallel to a measurement plane. It can be applied in different kind of flows in various micro scale flows. This method visualize the movement of a gas or a liquid by adding small tracer particles to the flow. Advance camera is used to capture the position of the particles with time lag between the images. JPIV is used for tracking the movement of the particles and correlates the movement of large number of red blood cells in order to visualize the result, fact that provides higher reliability concerning other [3]. It represents the most likely velocity of a tracer within an interrogation window.

The microscope used was a BX51 OLYMPUS System, illuminated by a pre-centered 12V100WHAL PHILIPS 7724 halogen lamp. A 50x objective was used, which in combination with the ocular lens magnification provided a magnification of 0.32 microns per pixel. An IDT XS-3 CMOS camera with a 1260x1024 pixel array was used for imaging.

2.3 The optical shearing software

A schematic description of the optical shearing system and the integrated camera and microscope is provided in Figure 13.

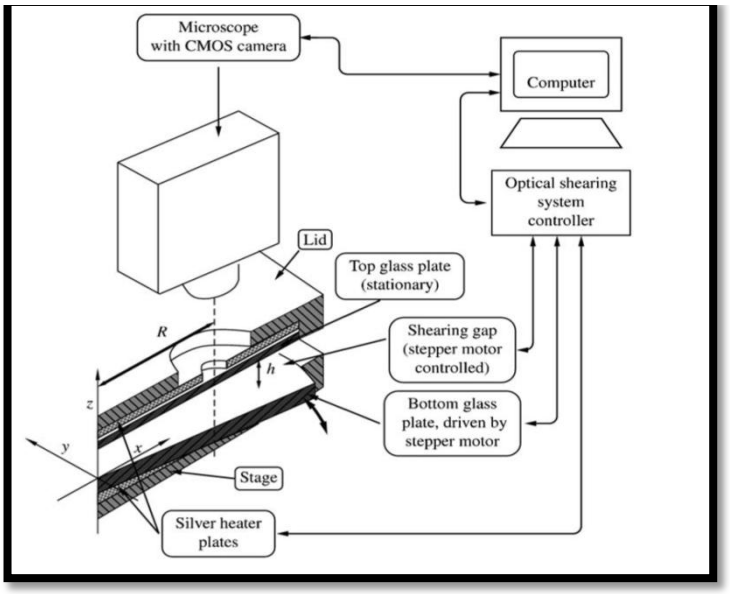

Figure 13. Schematic and experimental apparatus including the system and basic geometry variables [3]

Detail of the configuration of the optical shearing system is shown in detail in Fig.13. It consisted of two glass plates separated by a gap h=30 μm. The plate was sliding on the silicon tape, which was used to create the additional wall. The silicon material was adhered in the top plate and it was in contact with the bottom wall, sliding on it (please see Figure 14 for a top view of the configuration, corresponding to the schematic of Figure 13). The temperature was maintained at 37^{o}C [3]. The lower plate was driven by a stepper motor to shear the blood in the z direction with a nominal shear rate γ that was controlled by the lower plate rotational velocity ω. The centre of the viewing window located at a radius R=7.5mm from the plate axis of rotation, so the nominal shear rate across the gap is given by $\gamma=\omega R/h$. The samples were subjected to different nominal shear rates (2.5, 5.4, 11.2, 25.4, 33.1, 54 s^{-1}).

The coordinate system used in the present study is illustrated in Figure 14 below, on a representative image for blood flow in the plate-plate geometry of Figure 13. Note that the cross-flow direction will be indicated with either x or r (radial direction) in the following analysis.

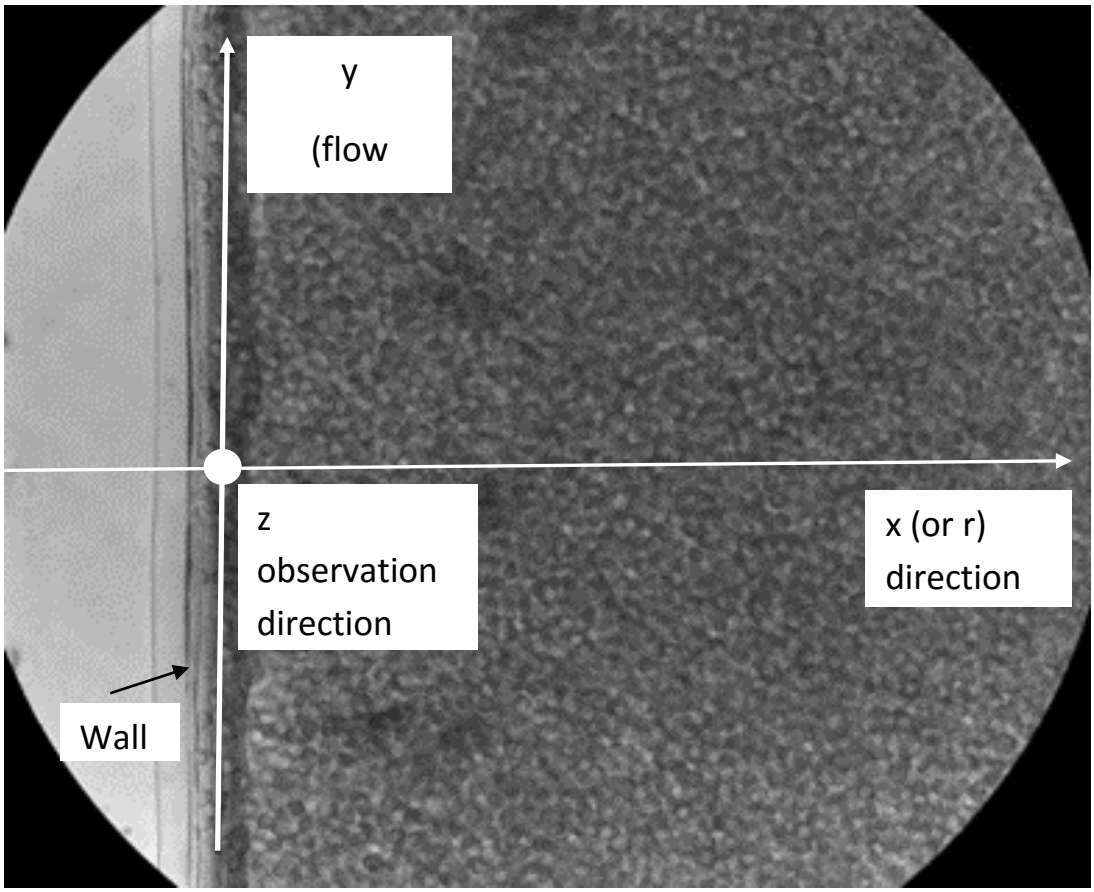

Figure 14. The coordinate system illustrated on a representative image for blood flow in the plate-plate geometry of Figure 13. Note that the cross-flow direction will be indicated with either x or r (radial) in the following analysis.

2.4 Aggregation index

For the purpose of measuring the intensity of aggregation in the fluid an aggregation index was developed based on the standard deviation (STD) of pixel grayscale intensity values. The STD indicates the amount of dispersion about the mean values. The aggregation index was defined as the coefficient of variation:

$$CV = \frac{STD}{Mean\ Velocity} \qquad (20)$$

STD=Standard deviation

CV=coefficient of variation

Minimum aggregation is achieved when STD value is minimum, therefore at low CV values. A high CV value would indicate increased aggregation. Image processing with matlab algorithms were used in order to calculate CV and characterize the phenomenon of aggregation.

2.5 The analytical solution for flow between plates with an extra boundary

The flow of a Newtonian fluid in the geometry used in the present study could be approximated by considering the analytical solution derived by the Navier-Stokes equations. For this purpose the flow is approximated as a fluid confined in low aspect ratio rectangular geometry having two adjacent sides (the side-wall and the top boundary) with zero velocity, the bottom wall at a constant velocity, and the wall as x tends to infinity at zero velocity also. Figure 15 illustrate the geometry and the flow conditions.

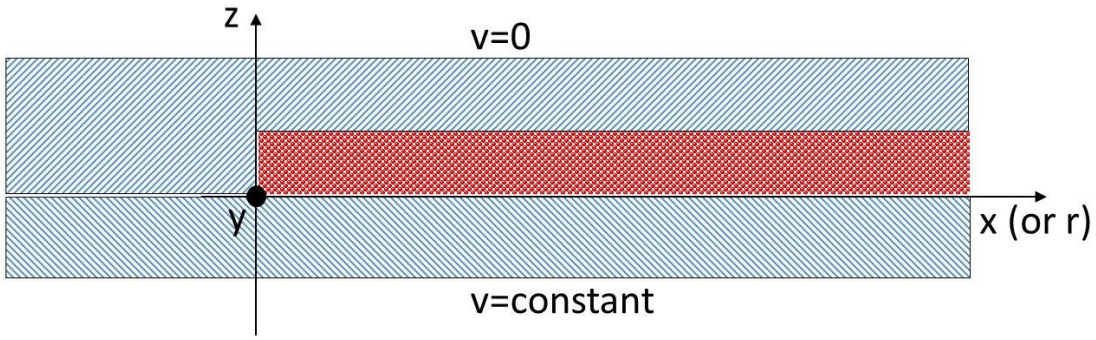

Figure 15. Schematic representation of geometry. The bottom plate was sliding on the silicon tape which was adhered in the top plate.

The development of the solution is based on Boas [27]. The equations to describe the flow are the 3D NAVIER-STOKES equations:

$$p\left(\frac{\partial u}{\partial t}+u\frac{\partial u}{\partial x}+v\frac{\partial u}{\partial y}+w\frac{\partial u}{\partial z}\right)=-\frac{\partial P}{\partial x}+pg_x+n\left(\frac{\partial^2 u}{\partial x^2}+\frac{\partial^2 u}{\partial y^2}+\frac{\partial^2 u}{\partial z^2}\right)$$

$$p\left(\frac{\partial v}{\partial t}+u\frac{\partial v}{\partial x}+v\frac{\partial v}{\partial y}+w\frac{\partial v}{\partial z}\right)=-\frac{\partial P}{\partial y}+pg_y+n\left(\frac{\partial^2 v}{\partial x^2}+\frac{\partial^2 v}{\partial y^2}+\frac{\partial^2 v}{\partial z^2}\right)$$

$$p\left(\frac{\partial w}{\partial t}+u\frac{\partial w}{\partial x}+v\frac{\partial w}{\partial y}+w\frac{\partial w}{\partial z}\right)=-\frac{\partial P}{\partial z}+pg_z+n\left(\frac{\partial^2 w}{\partial x^2}+\frac{\partial^2 w}{\partial y^2}+\frac{\partial^2 w}{\partial z^2}\right)$$

The z and x velocity components been negligible the Navier-Stokes equations reduce to the following:

$$p\left(\frac{\partial v}{\partial t}+u\frac{\partial v}{\partial x}+v\frac{\partial v}{\partial y}+w\frac{\partial v}{\partial z}\right)=-\frac{\partial P}{\partial x}+pg_x+n\left(\frac{\partial^2 v}{\partial x^2}+\frac{\partial^2 v}{\partial y^2}+\frac{\partial^2 v}{\partial z^2}\right)$$

For the steady and fully developed flow there are no changes in time, and in the particular case, no changes in pressure are present. According to Figure 15 no changes of the velocity (u) in the x direction, and therefore only changes in y and z directions are expected due to the boundaries of the system. Therefore the equation reduces to:

$$n\left(\frac{\partial^2 v}{\partial x^2}+\frac{\partial^2 v}{\partial z^2}\right)=0$$

$$\frac{\partial^2 v}{\partial x^2}+\frac{\partial^2 v}{\partial z^2}=0 \quad (1)$$

That means that the velocity depends on y and z

$$\mathrm{v(x,z)}=Y(x)Z(z) \quad (2)$$

We indicate that Y is a function of x and Z is a function only of z. If we have the solutions for Y and Z then according to equation (2) we can combine them to get the solution we want for u. Substituting the (2) into (1) we have

$$Z\left(\frac{\partial^2 Y}{\partial x^2}\right)+Y\left(\frac{\partial^2 Z}{\partial z^2}\right)=0 \quad (3)$$

Divide (3) by YZ to get

$$\frac{1}{Y}\frac{\partial^2 Y}{\partial x^2}+\frac{1}{Z}\frac{\partial^2 Z}{\partial z}=0 \qquad (4)$$

The above analytical solution is the Steady State Laplace Equation. For the specific geometry the calculation of the velocity in a Rectangular Plate (two adjacent plates equal to zero velocity and the other plate with constant velocity) is required.

The next step is to solve the equation by separation of variables. Each of the terms in (4) is a constant because the first term is a function of y alone and the second one is a function of z alone. From (4) we the write

$$\frac{1}{Y}\frac{\partial^2 Y}{\partial x^2}=-\frac{1}{Z}\frac{\partial^2 Z}{\partial z}=-constant=-k^2 \qquad k\geq 0 \quad (5)$$

The solution of (5) is given when considering flow conditions:

$$\text{Y} \begin{cases} \sin kx \\ \cos kx \end{cases} \qquad \text{Z} \begin{cases} e^{kz} \\ e^{-kz} \end{cases} \qquad (6)$$

The solution to equation (1) will be a combination of the above solutions:

$$\text{v(x, z)} = Y(x)Z(z) = \begin{cases} \sin kx \\ \cos kx \end{cases} \begin{cases} e^{kz} \\ e^{-kz} \end{cases} \qquad (7)$$

The constant k of the solutions in (7) should satisfy the given boundary velocities. We take a combination of the solution (7), with the constant k properly selected, which will satisfy the given boundary conditions; we first need a condition to give v=0 for z = 30microns (the height of the configuration). This is possible by combining the e^{kz} terms: $\frac{1}{2}\text{e}^{\text{k(30-z)}} - \frac{1}{2}\text{e}^{-\text{k(30-z)}}$. By identity tis is sinh(k(30-z)). Next we discard solutions containing cosky since v=0 when y=0. This leaves us just V=sinh(k(30-z))*sin(kx), but the value of k is still to be determined.

At a large value of x (xinf) we have v=0; this will be true if sin(xinf k)=0; that is, if $k = \frac{n\pi}{\text{xinf}}$ for n=1,2, ... Thus for any integral n, the solution

$$\text{V} = \sinh\left[\left(\frac{\text{n}\pi}{xinf}\right)(30 - \text{z})\right] * \sin\frac{n\pi x}{xinf} \qquad (8)$$

The solution (8) satisfies the boundary conditions for all n, however the condition that at z=0, V=Vplate, still needs to be satisfied. Therefore:

$$\text{V} = \sum_{\text{n}=1}^{\infty} \text{b}_\text{n} \sin\frac{\text{n}\pi x}{\text{xinf}} = \text{Vplate} \qquad (9)$$

That is we must have V=specific magnitude when z=0. This condition is not satisfied by (8) for any n. But a linear combination of solution (8) is a solution of (1). For z=0 we must have specific U from (9) with z=0 we get.

$$\text{Vplate} = \sum_{\text{n}=1}^{\infty} \text{b}_\text{n} \sin\frac{\text{n}\pi x}{\text{xinf}} \qquad (10)$$

Now we can find coefficient b_n from:

$$b_n = \frac{2}{x}\int f(x) * \sin\frac{n\pi r *}{x}\partial x = \frac{2}{xinf}\int Vplate * \sin\frac{n\pi x}{xinf}\,\partial x \qquad (11)$$

With limits from 0 to xinf the solution is:

$$\begin{cases} \frac{4\ \text{Vplate}}{n\pi} & \text{odd n} \\ 0 & \text{even n} \end{cases}$$

The complete solution for the Newtonian flow in the present geometry:

$$v = \sum_{n=1}^{\infty} \frac{4\ Vplate}{n\pi}\ \frac{\sin h\left(\frac{n\pi}{xinf}(30 - z)\right)}{\sin h\left(\frac{n\pi 30}{xinf}\right)}\ \sin\left(\frac{n\pi x}{xinf}\right) \qquad (13)$$

CHAPTER 3. RESULTS

In this chapter we will be presented and discussed the velocity and aggregation behavior of red blood cells flowing between the plate-plate geometry near an extra boundary (geometry in Figure 15). Three different cases will be examined: a non-aggregating (PBS) and two aggregating samples (Dextran 70 and 2000) subjected to different shear rates (2.5, 5, 11, 25, 33 and 54 s^{-1}). The velocity will be presented as absolute V and normalized ($V^* = v/vmax$) values against normalized radius, where gap can be define as 30μm($r^* = r/gap$). Furthermore the local shear rates will be presented as calculated from the derived velocity fields. An attempt to quantify the aggregation behavior will be made using the standard deviation of velocity and grayscale image intensity values as aggregation indices.

Figure 16 below shows representative images for non-aggregating (PBS) and aggregating (D70 and D2000) samples in the plate-plate shearing system. As it can be seen the phenomenon of aggregation influences significantly the structure of the fluid, especially at the lower nominal shear rates.

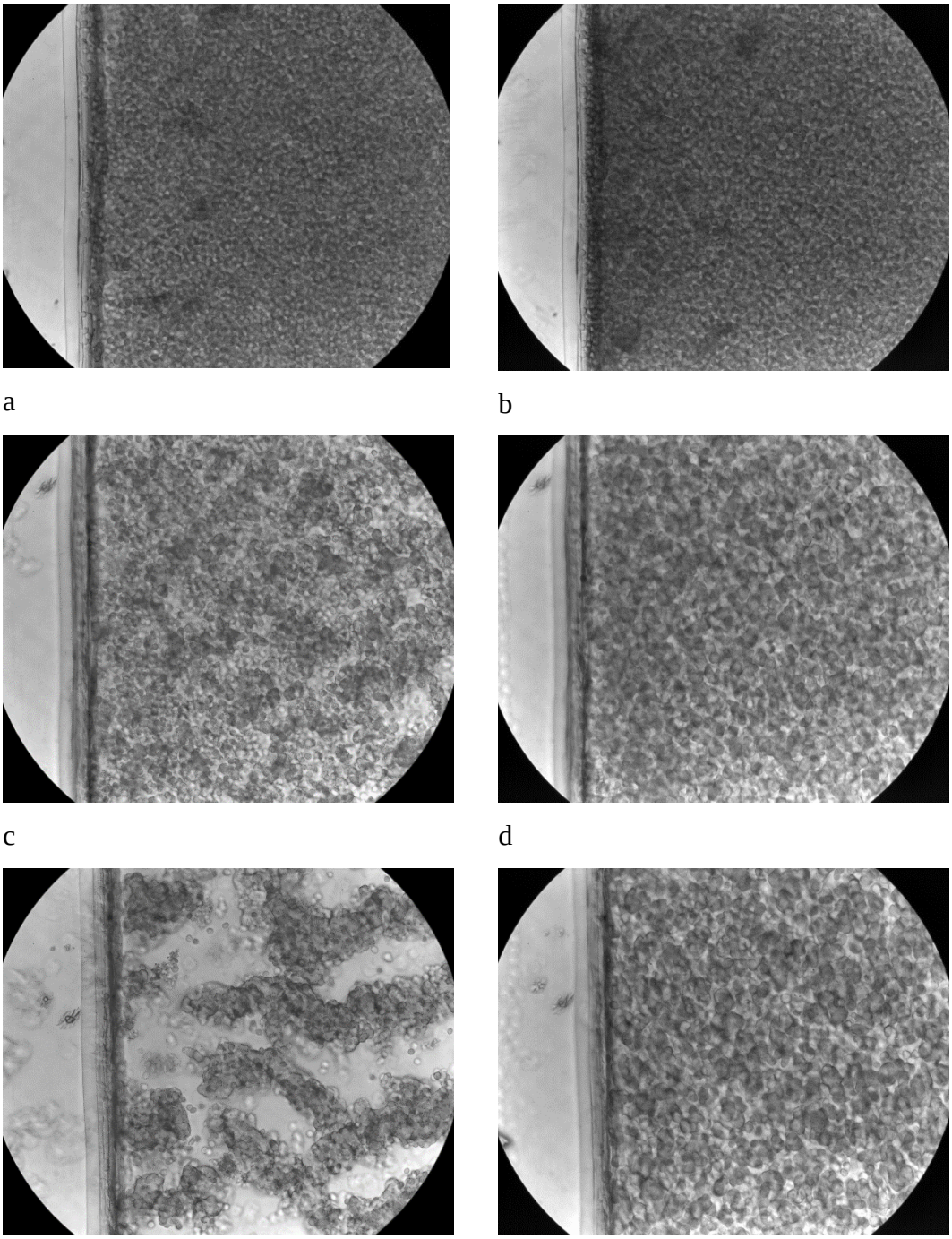

Figure 16. Representative images of blood flow for different aggregative states and at low and high nominal shear rates. a and b: PBS case at 2.5 and 54 s^{-1} respectively. c and d: D70 case at 5 and 54 s^{-1} respectively. e and f D2000 case at 5 and 54 s^{-1} respectively.

3.1 Velocity analysis

This section is concerned with the examination of the velocity characteristics as developed in the fluid by the motion of the bottom plate and as they are influenced by the aggregation tendency of the cells. For this purpose the following analysis has been performed:

- Analysis of the JPIV data (not-scaled velocity) and the standard deviation for 50 images
- Analysis of the normalized JPIV data with the maximum velocity in each data set
- Analysis of the absolute values of velocity against the nominal shear rates (please see section 2.3 for the definition of nominal shear rate)

3.1.1 Velocity profiles and STD for PBS

The initial analysis is focused on examining the values of not-scaled velocities and the standard deviation for each value in the r* direction. As the PIV data are not scaled the values of velocity presented in this section represent distance (in pixels) covered per frame. The data will be presented against the normalized radius r*.

Figure 17(a) shows the velocity data (mean values from 50 processed images) against r* for the PBS cases and for nominal shear rates of 2.5, 33 and 54 s^{-1}: the values of the velocities at r*~11 are 0.7, 2 and 2.5 respectively for each of the aforementioned cases. The standard deviation values for the PBS cases are presented in Figure 17(b): observed values at r*~11 are 0.5, 2.5 and 1.8 for the shear rates of 2.5, 33 and 54 s^{-1} respectively.

In the graph of Figure 17(a) it is observed that as the shear rate is increased so the velocity does. There is also a trend between the cases; as we move away from the side wall we observe that the velocity increases. In addition near the wall the velocity tends to be close to zero. Away from the wall the profile tends to be smoother and flatter. For the case of $2.5s^{-1}$ the velocity of the cells is expected to follow the velocity of the plate due to the sedimentation of the cells. Increasing the shear rate contributes to an increase in cell size. Furthermore with increasing shear rate is observed that there is no noticeable change due to the lack of data.

In Figure 17(b) is observed that the magnitude of STD increases as the shear rate is increased. This indicates that the data for the low shear rates tend to be closer to the mean value so there is small dispersion of data in comparison to the higher shear rates. The STD for the shear rate $33s^{-1}$ and $54s^{-1}$ behaves similarly; higher STD indicates higher spread of the data. The frame rate (FR) which was used for PBS it was 100 for $2.5s^{-1}$, and 400 for the cases of $33s^{-1}$ and $54s^{-1}$. The increase of the FR is necessary because of the increase of the velocity of the particles; this would ensure better quality of images providing more accurate results from the JPIV analysis.

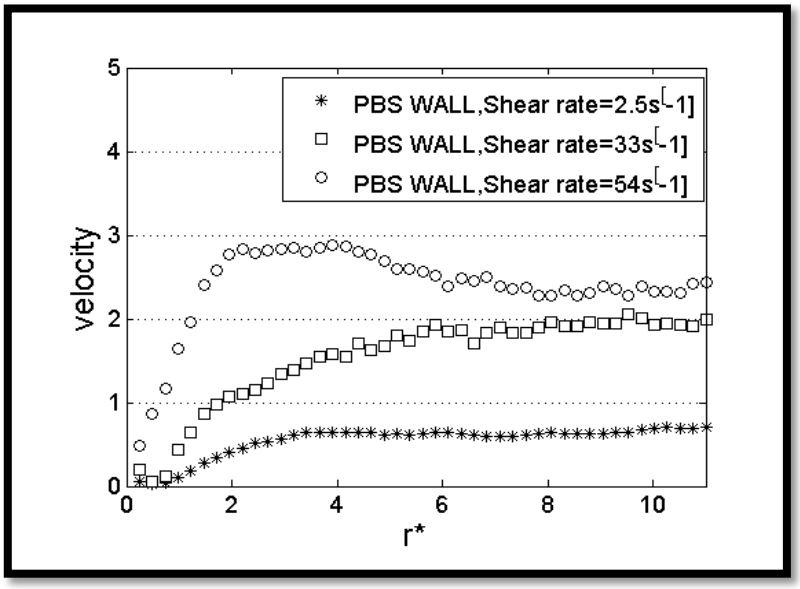

a

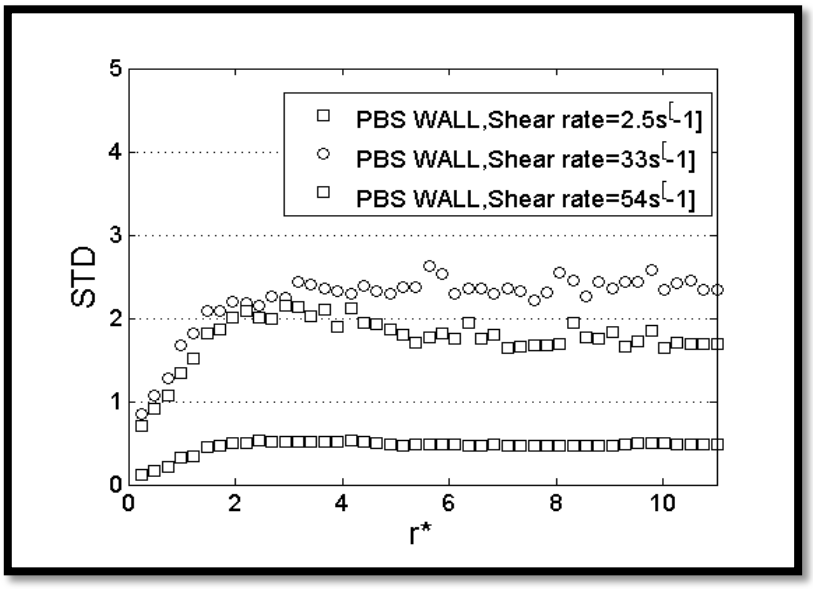

b

Figure 17. a) the velocity profile against r*and b) the standard deviation of PBS cases under different shear rates

3.1.2 Velocity profiles and STD for D70

Figure 18(a) shows the velocity behavior of D70 against r* for different cases : 1,5,11,25 and 54 s^{-1}. The velocity data was measured by the mean values from 60 processed images.

In figure 18(a) is observed low values of velocities at low shear rate, and proportionally at high shear rate , high values of velocity. There is trend between the high shear rate and the low shear rate. The explanation for the wall slip condition is confirmed; near the wall the velocity tends to be close to zero. Moving away from the wall the velocity increases and the profile tends to be smoother. An interesting pattern is observed for the case of $1s^{-1}$ and $5s^{-1}$ the velocity of the cells follow the velocity of the plate due to sedimentation of the cells. Furthermore from some shear rates we do not observe changes due to lack of data. For nominal shear rates of 1, 5, 11,25 and 54 s^{-1},the values of the velocities at r*~11 are 1 , 3.4 ,7, 8.5 and 7 respectively for each of the aforementioned cases.

In Figure 18(b) is presented the magnitude of STD against r* for the D70 cases: 1,5,11,25 and 54 s^{-1} .In the specific graph the amount of STD for the lower shear rate of $1s^{-1}$ is the maximum. In this figure is observed that the values at r*~11 are 3, 0.8, 1.2 , 2.5 and 5 for the shear rates of 1, 5, 11, 25 and 54 s^{-1} respectively. The frame rate which was used for D70 it was 100 for $1s^{-1}$, $5s^{-1}$, $11s^{-1}$,200 for $25s^{-1}$and 400 for the case of $54s^{-1}$.

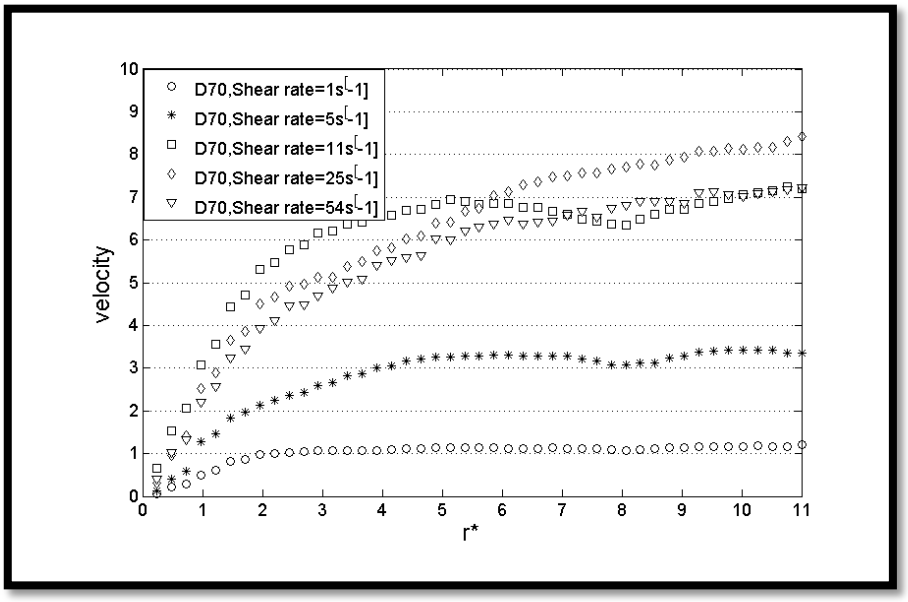

(a)

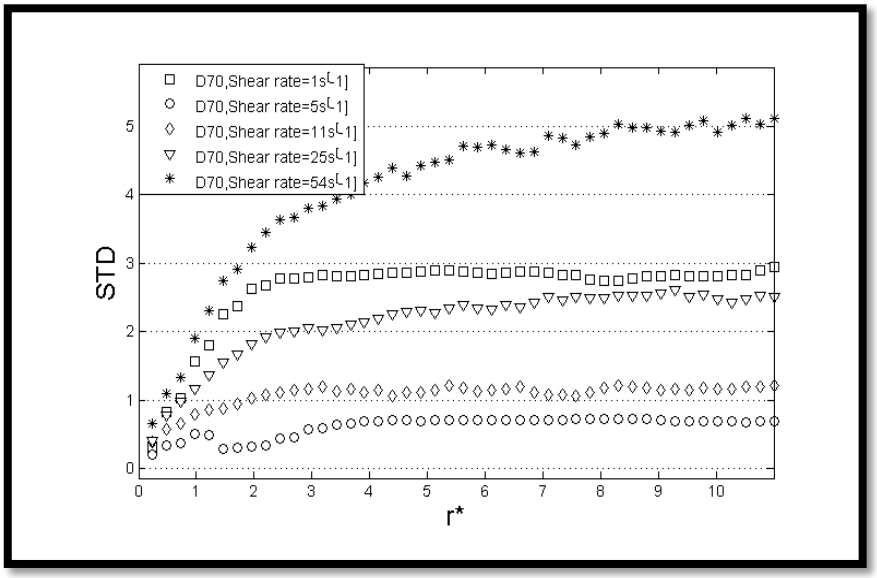

(b)

Figure 18. a) the velocity profile against radius gap, b) the standard deviation of D70 under different shear rates

3.1.3 Velocity profiles and STD for D2000

Figure 19(a) shows the velocity behavior of D2000 under different shear rates. The behavior is presented in a graph of velocity values (mean values from 100 processed images) against r* for the D2000 cases and for nominal shear rates of 5, 11,25 and 54 s^{-1}: the values of the velocities at r*~11 are 3, 7 and 9 respectively for each of the aforementioned cases.

In the graph 19(a) is observed that the shear rate is increased accordingly ; at low nominal shear rate are observed low values of velocity and at the high shear rate ,higher values of velocity. The general behavior of velocity is similar to the previous cases: away from the plate the velocity increases, and the profile tends to be smoother and flatter. In addition near the wall the velocity tends to be close to zero. The maximum velocity, is observed at maximum shear rate 54 s^{-1} and the minimum at low shear rate $5s^{-1}$. Furthermore from some shear rates we do not observe changes due to lack of data.

In Figure 19 (b) is presented the standard deviation values for the D2000 shear 5, 11,25 and 54 s^{-1} . The STD graph is the way that we can quantify the dispersion of a set of velocity data .In this figure is observed that the values at r*~11 are 1.5,1, 2.5

and 4 for the shear rates of 5, 11,25 and 54 s^{-1} respectively. The magnitude of STD increases as we increase the shear rate. The STD for the shear rate $5s^{-1}$ and $11s^{-1}$ behaves similarly. The frame rate (FR) which was used for D2000 it was 30 for $5s^{-1}$, 200 for $11s^{-1}$, 200 for $25s^{-1}$, and 400 for $54s^{-1}$ as necessary because of the increase of the velocity of the particles.

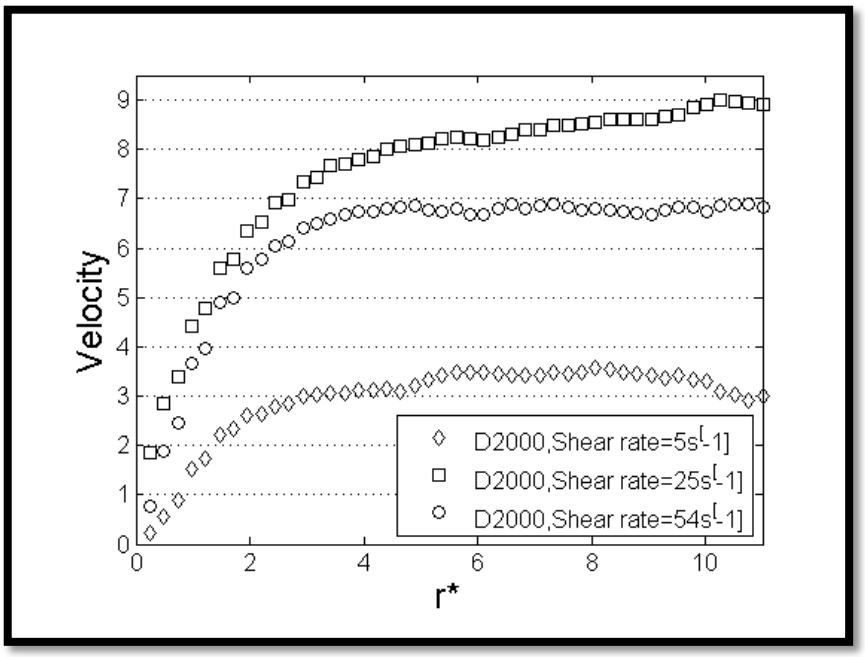

(a)

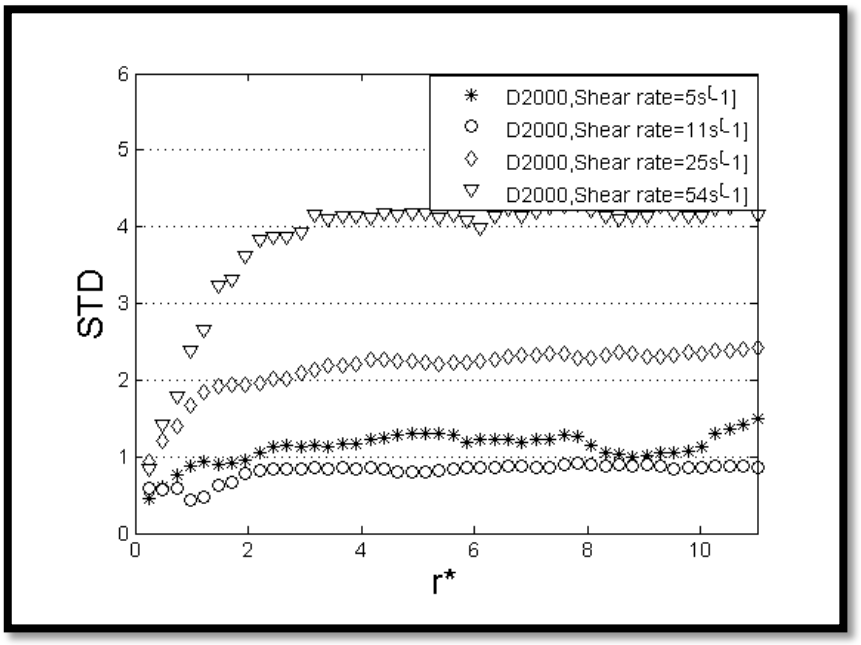

(b)

Figure 19. a) the velocity profile against radius gap, b) the standard deviation of D2000 under

different shear rates

3.1.4 STD profile comparison at similar shear rates

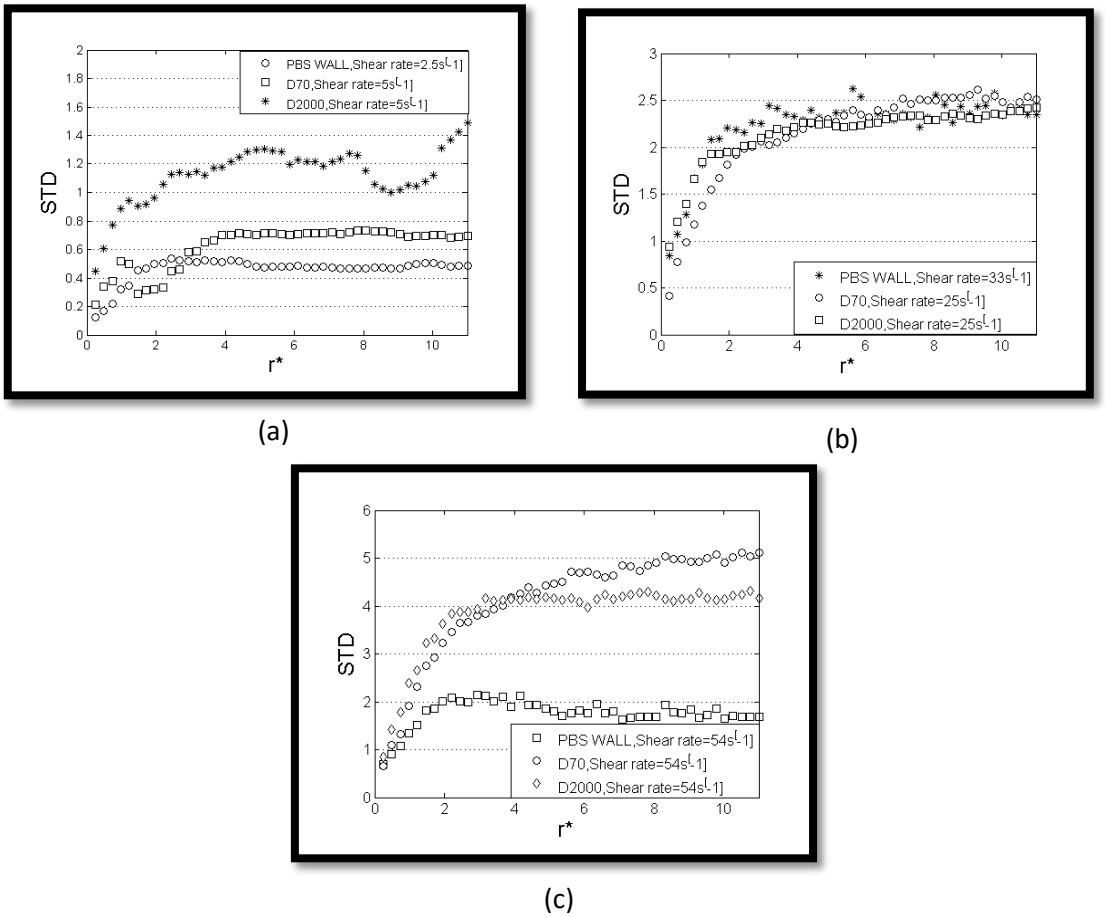

Figure 20 The standard deviation for the PBS, D70 and D2000 cases for the nominal shear rates 2.5 and 5s^{-1} (panel a), 25 and 33s^{-1} (panel b) and the 54s^{-1} case.

In Figure 20(a) is presented the STD profiles for PBS ,D70 and D2000 cases for the lower nominal shear rates (2.5 to 5s^{-1}) against normalized radius r*. It is observed that the magnitude of STD for the PBS case is lower than the D70 and D2000 cases. The maximum STD is observed at the D2000 case. This indicates that the data dispersion in the lower nominal shear in the PBS case tends to be close to the mean. There is a trend apparent that is as we moving from PBS (non-aggregation case) to the Dextran cases the STD is increasing.

In Figure 20(b) is presented the STD profile of PBS ,D70 and D2000 for shear rate of 25s^{-1}.The behavior of the STD in this case is observed to be similar: the maximum STD is observed at r*~11 in contrast to the PBS case. We would expect to have

similar behavior for D70 and D2000 and at PBS, as the cells at this case don't aggregate resulting in lower STD.

For the higher shear rate of 54 in Figure 20(c) the magnitude of STD for the PBS is lower than D70 and D2000. The maximum STD is observed in the D70 case at r*~11. Again a trend is observed as we moving from PBS (non-aggregation case) to Dextrans. Our expectations for similar behavior for the Dextrans is confirmed. The PBS , the non-aggregation case, has lower STD than Dextrans.

3.1.5 Normalized velocity profiles for the PBS cases

For a more thorough analysis and better comparison of the qualitative characteristics of the velocity behavior between the cases, the PIV data were normalized with the maximum values occurring in each velocity profile.

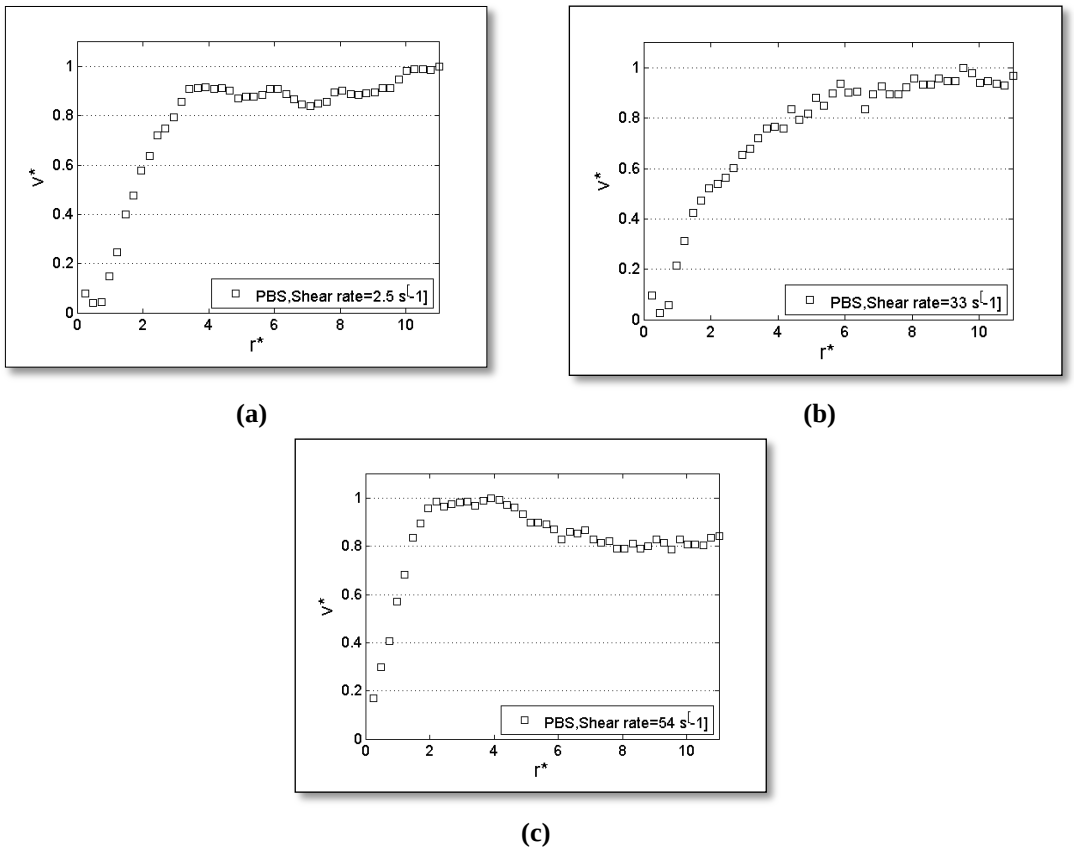

Figure 21. Velocity profiles for the PBS cases (a) Velocity profile for shear rate of 2.5s^{-1} (b) Velocity profile for shear rate 33s^{-} (c) Velocity profile for shear rate 54s^{-1}

In Figure 21(a) is presented the velocity behavior of RBCs for the PBS case and for the shear rates of 2.5s^{-1}, 33s^{-1} and 54s^{-1}. The behavior of the velocity (V^*) for the PBS case is presented in the graph against the normalized radius(r^*). It should be noted

there is unevenness at the wall due to the adhesive of the silicon sheet, and therefore the flow is more complex in the region very close to the side walls. We would expect to get zero velocities at the side wall, however there is a slip effect since RBCs tend to move away from the boundaries. Another observation is that away from the wall the velocity profile becomes more smooth and flat. Another distinctive characteristic is that at the $2.5s^{-1}$ shear rate the highest V^* close to the wall occurs at $r^* \sim 3.75$ and the minimum V^* close to the wall is at $r^* = 0.5$. Moreover the highest V^* away from the wall is at $r^* > 10$, and the graph is getting flatter at $r^* > 3.75$.

In Figure 21(b) is presented the velocity behavior for the $33s^{-1}$ case; the behavior the velocity in this case is similar to the $2.5s^{-1}$: Low velocities are observed closed to the wall, increasing as r^* increases and reaching a maximum at around $r^* = 4$. In addition the minimum V^* close to the wall is observed at $r^* = 0.5$. Moreover the highest V^* away from the wall is at $r^* > 9$, and the velocity stabilized at approximately $r^* = 4$.

In figure 21(c) is presented the behavior of velocity for the case of shear rate $54s^{-1}$. The velocity at this shear rate behaves differently from the other cases ($2.5s^{-1}$ and $54s^{-1}$): the velocity reaches the highest value at $r^* \sim 2$. The slip due to RBCs tendency to move away from the wall is also apparent in the figure. Away from the wall the velocity profile becomes more flat at around $r^* = 2$. The minimum V^*close to the wall is at r*=0.05 .

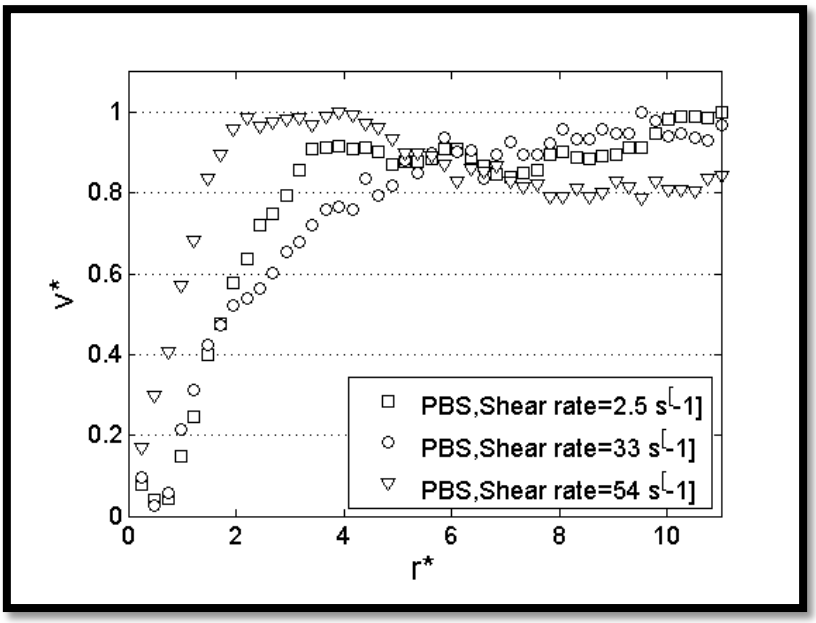

Figure 22. Velocity profiles for PBS WALL comparison shear rates

In Figure 22 is presented the velocity behavior of all the PBS cases. The behavior of velocity at shear rates $2.5s^{-1}$, and $33s^{-1}$ is similar: close to the wall we observe small velocities increasing as r^* increases and reaching a maximum at around $r^* = 0.5$. On the other hand the behavior of $54s^{-1}$ close to wall is different, possibly due to lower sedimentation occurring in the flow; at high shear rates the cells are better distributed in the flow (see Figure 22) and they do not sediment easily. No trends are observed between different shear rates close and away from the wall, where the velocity profile becomes more smooth for all the shear rates.

The PBS cases can be considered closer to the Newtonian case as the aggregation effects are not apparent in the flow. For this reason the analytical solution has been produced and shown in Figure 23. In the figure the expected behavior of velocity is illustrated.

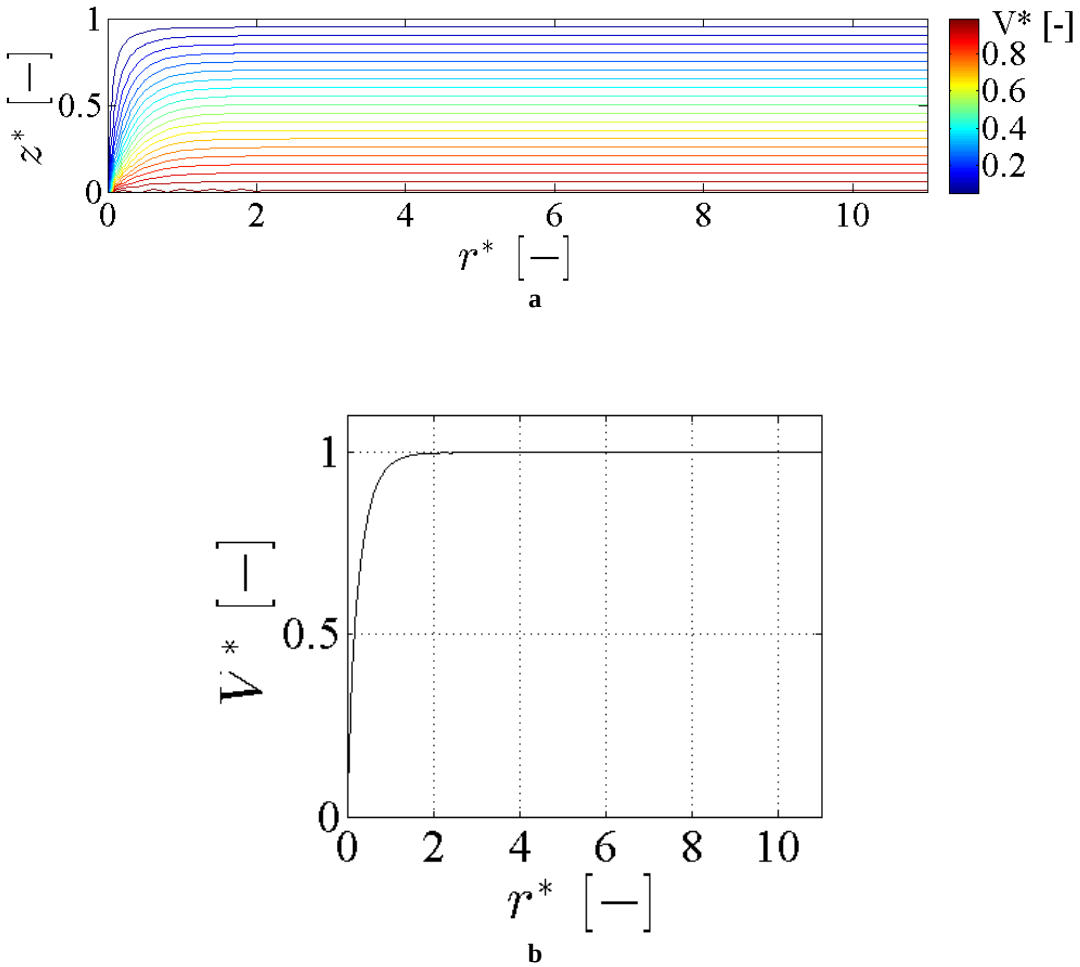

Figure 23. Velocity profiles for the PBS case: a) the velocity distribution in the z-x (z-r*) plane. Here the x axis is presented in terms of radius r; both the z and r directions are normalized by the gap of the geometry. b) the mean velocity profile in the z direction.

The velocity in the analytical solution shown in Figure 23 is normalized as in the experimental cases. In Figure 23(b) is shown the velocity averaged in the z direction. The most significant difference between the theoretical solution and the experimental data for the PBS case is the quality of the graphs. The theoretical solution graph is smoother than the experimental graph, and can be described qualitatively.

3.1.6 Normalized velocity profiles for the aggregating cases (D70)

For the aggregating samples (D70 cases) experiments performed at 5 different cases (shear rates of $1s^{-1}$, $5s^{-1}$, $11s^{-1}$ and $25s^{-1}$ and $54s^{-1}$) and the results are shown in Figure 24 below. Similarly to the previous cases the behavior of velocity presented as normalized velocity (V^*) against normalized radius (r^*) . The effects of the unevenness at the vertical wall due to the adhesive of the silicon sheet seem minimized in the present cases, possibly due to the different aggregation intensity induced by the Dextran 70. The slip effect at the wall is also apparent in the present cases and no zero velocities where observed at r*=0. Away from the wall the velocity profile becomes more smooth and flat.

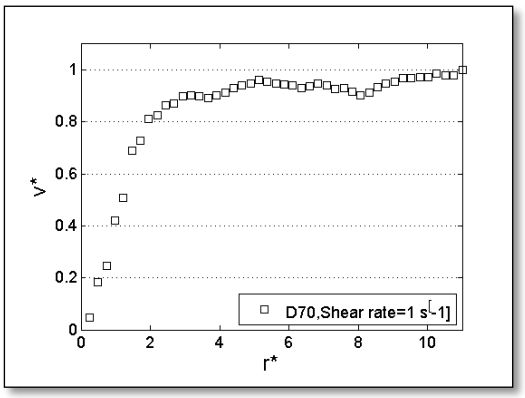

(a)

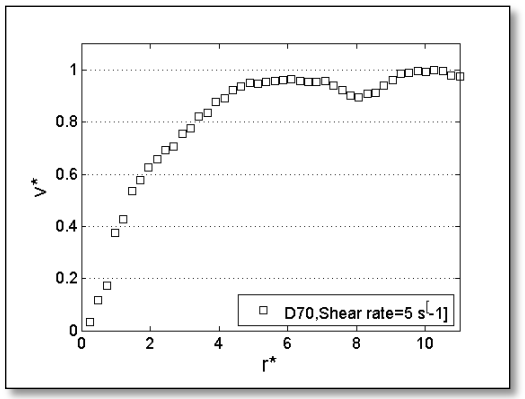

(b)

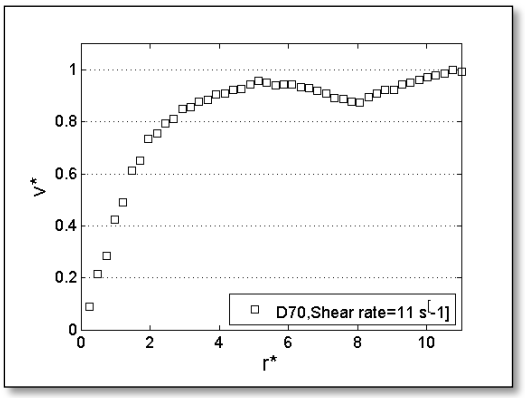

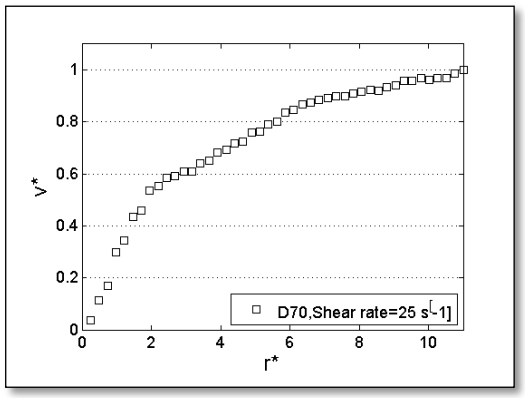

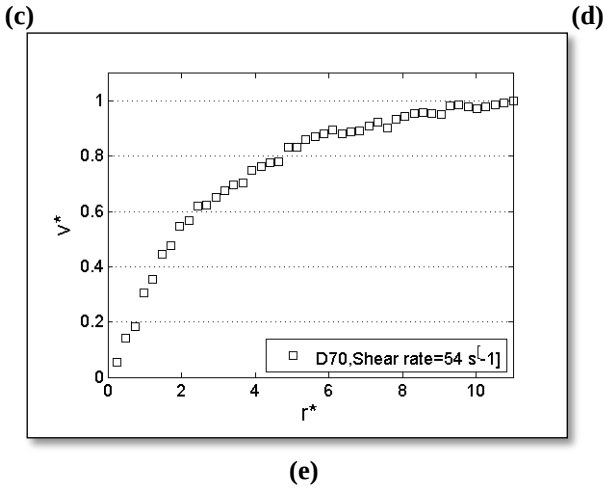

Figure 24. Velocity profiles for the cases D70 (a) Velocity profile for shear rate $1s^{-1}$ (b) Velocity profile for shear rate $5s^{-}$ (c) Velocity profile for shear rate $11s^{-1}$ (d) Velocity profile for shear rate $25s^{-1}$ (e) Velocity profile for shear rate 54 s^{-1}

More specifically, for the shear rate of $1s^{-1}$, V^* reaches highest values(near the wall) at approximately $r^* = 3$. The velocity reaches its maximum value at $r^* = 11$, and the graph getting flatter after $r^* = 2.5$. For the velocity behavior for the $5s^{-1}$ case (in Figure 24(b)) the behavior of V* is similar to the $1s^{-1}$: small velocities are observed closed to the wall increasing as r^* increases and reaching a maximum at around $r^* = 10$. At the shear rate of $5s^{-1}$ the velocity gains high V^* values after approximately $r^* = 4$. The reaches a plateau after $r^* = 4$. Figure 24(c) shows the case of shear rate $11s^{-1}$ which is similar to the previous cases: the highest V^*near the wall is reached at $r^* = 2$ where the graph gets flatter. Again no zero velocities are apparent due to the wall slip phenomenon and the velocity reaches its maximum value at $r^* = 11$.

In Figure 24(d) is presented the velocity behavior for the $25s^{-1}$ case. The highest V^* close to the wall is at $r^* = 3$ .In addition away from the wall the velocity profile becomes more smooth. In addition the minimum V^*close to the wall is at r*=0.01. Moreover the highest V^* away from the wall is at $r^* = 11$, and the graph get flat at $r^* = 3$. For the case of $54s^{-1}$ (Figure 24(e)) the highest V^* close to the wall is at $r^* = 3$, the maximum V^* is at $r^* = 11$, and the graph gets flat at $r^* = 3$. In addition the minimum V^*close to the wall is at r*=0.01 due to the wall slip phenomenon; zero velocities near the wall. The case of $54s^{-1}$ is smoother than the other cases of D70.

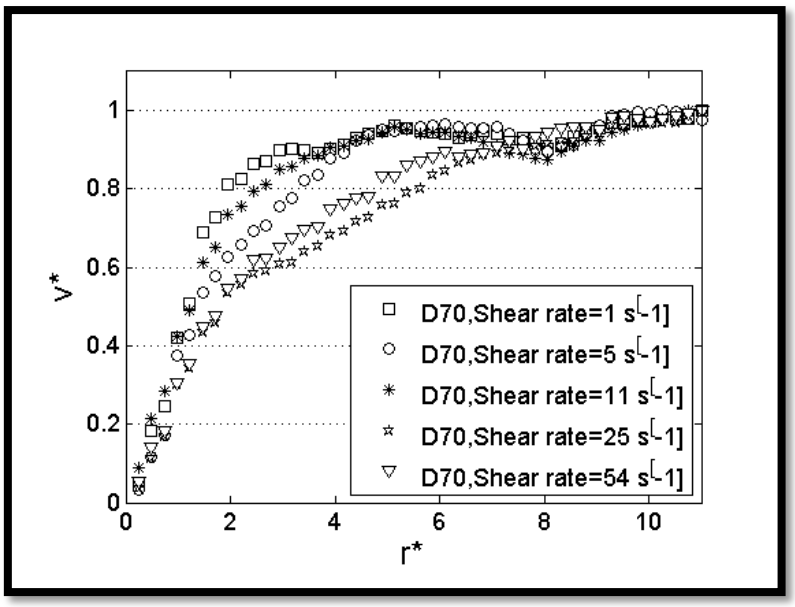

Figure 25. Velocity profiles for D70 comparison shear rates

The velocity profiles from all shear rates tested in the D70 case are presented in comparison in Figure 25. An interesting pattern is observed in Figure 25; very similar behavior for r* between 0 and around 2 and between approximately 7 and 11. More interestingly a trend is observed for the velocities between r*= 2 and 7; the velocities in the smaller shear rates (e.g. in 1, 5 and 11) seem to develop faster than those in the higher shear rates (25 and 54 s^{-1}). This could be attributed to fact that at lower shear rates the cells sediment faster and a greater population of cells gain higher velocities from the rotating plate. Note that the maximum velocity occurs at the rotating plate.

3.1.7 Normalized velocity profiles for the aggregating cases (D2000)

The velocity behavior of RBCs for the D2000 case at 4 different shear rates ($5s^{-1}$, $11s^{-1}$, $25s^{-1}$ and $54s^{-1}$) is presented in Figure 26.

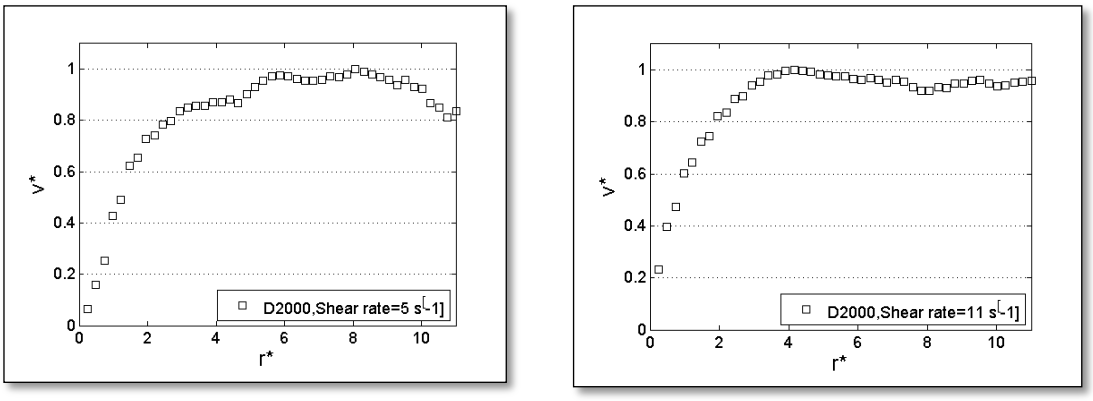

(a) **(b)**

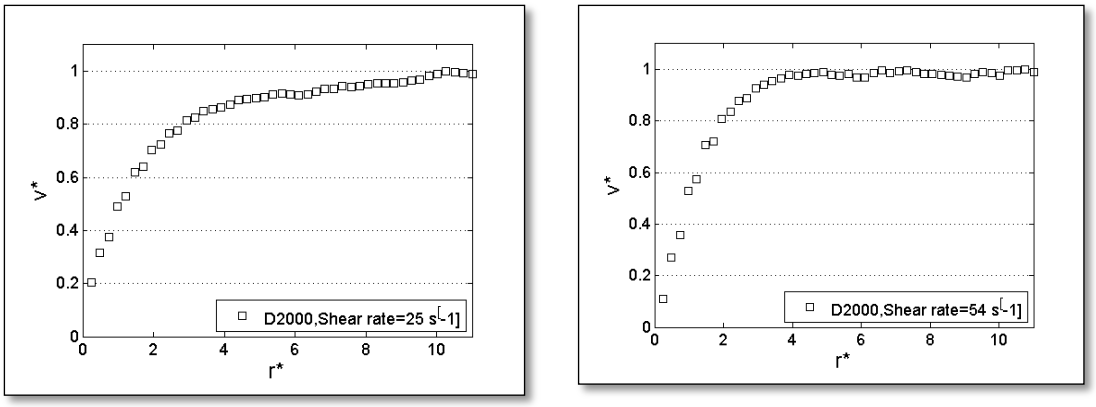

(c) **(d)**

Figure 26. Velocity profiles for the cases D2000 (a) Velocity profile for shear rate 1s^{-1}

(b) Velocity profile for shear rate 5s^{-} (c) Velocity profile for shear rate 11s^{-1} (d) Velocity profile for shear rate 25s^{-1} (e) Velocity profile for shear rate 54 s^{-1}

The general behavior of velocity is similar to the previous case; no zero velocities at the wall due to the slip condition, velocities increase with r* and reach maximum away from the wall.

In Figure 26(a) (5s^{-1}**)** the highest V^* close to the wall is at $r^* = 3$, the highest V^* away from the wall is at $r^* = 8$, and the graph gets flat at $r^* = 4$. In addition the minimum V^*close to the wall is at r*=0.01 due to the wall slip phenomenon. At the shear rate of 11s^{-1} in figure 26(b) the highest V^* on the gap is at $r^* = 4$. This means that the cells reaches the highest velocity value near the wall. The highest V^* near the wall for the 25 s^{-1} case (Figure 26(c)), is reached at $r^* = 3$ where the graph gets flatter. Again no zero velocities are apparent due to the wall slip phenomenon. Moreover the highest V^* away from the wall is at $r^* = 11$. In Figure 26(d) is presented the velocity behavior for the 54s^{-1} case: the highest V^* close to the wall is at $r^* = 3$ and the maximum V^* away from the wall is at $r^* = 7$. The velocity profile gets flatter at $r^* = 3$.

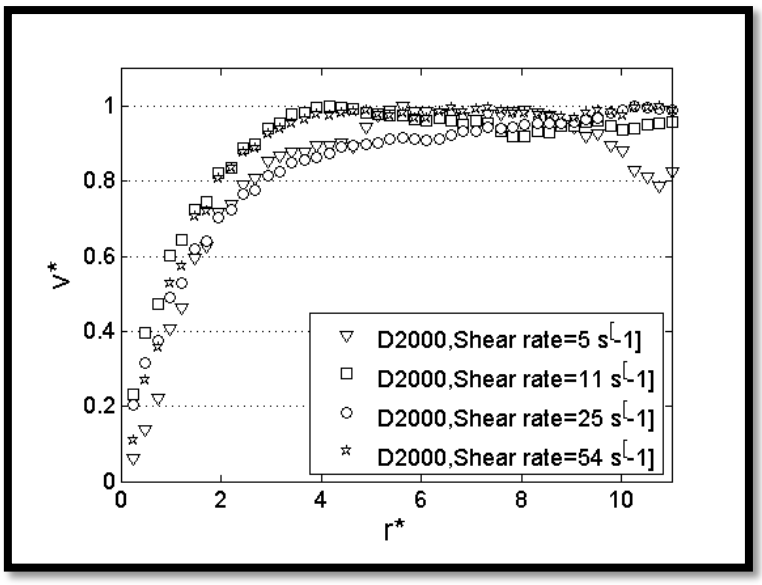

Figure 27. Velocity profiles for D2000 comparison shear rates

Velocity profiles for all the D2000 cases are plotted in comparison in Figure 27. The behavior of the velocities in all shear rates is similar: close to the wall we observe small velocities increasing as r^* increases and reaching a maximum at $r^* = 3$. Here the trend observed in Figure 25 (the D70 case) is not present.

3.1.8 Comparison of normalized velocities at similar shear conditions

3.1.8.1 Comparison of PBS, D70 and D2000 at 5s^{-1}

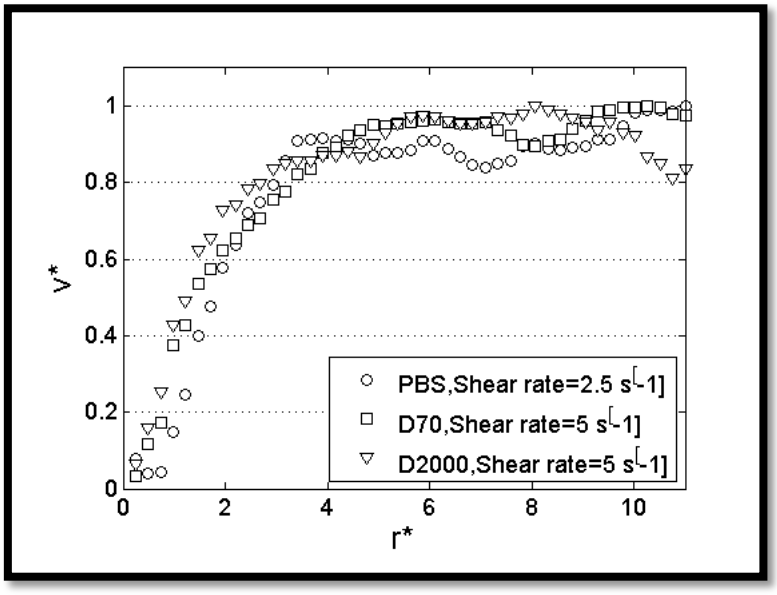

Figure 28.Velocity profiles for PBS WALL, D70, D2000 comparison graph at shear rate 5s^{-1}

In figure 28 is presented the velocity behavior of PBS ,D70 and D2000 for the nominal shear rate of 5s^{-1}. It is observed that at the first three points there are velocity

fluctuations possibly due to lower sedimentation occurring in the flow. No trends between the cases are observed. In addition near the wall (until $r^* = 3$) all the cases seems to behave similarly. At the end of geometry D2000 behaves differently; has lower V^* than the cases D70 and PBS. D70 and PBS reaches them maximum at r^* =11.

3.1.8.2 Comparison of PBS, D70 and D2000 at 25s^{-1}

Figure 29 shows the velocity behavior of PBS,D70 and D2000 for the nominal shear rate of 25s^{-1}. For this particular shear rate it is observed (Figure 29) that the PBS and D2000 cases behave similarly, however the D70 case seem to have a different behavior. No trends between the cases are observed.. At the end of geometry, D2000 and D70 behaves similarly; at r* is approximately 11 . PBS behaves differently; has lower V^* than the cases D70 and D2000.

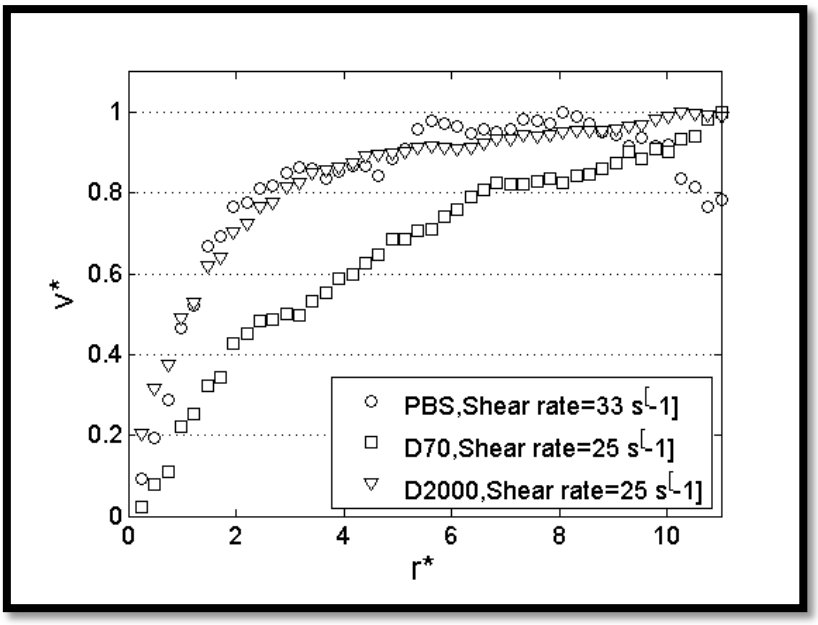

Figure 29. Velocity profiles for PBS WALL, D70, D2000 comparison graph at 33s^{-1}shear rate

3.1.8.3 Comparison of PBS, D70 and D2000 at 54s^{-1}

In figure 30 is presented the velocity behavior of PBS, D70 and D2000 for shear rate 54s^{-1}. The velocity is presented again as normalized velocity (V^*) against normalized radius(r^*).

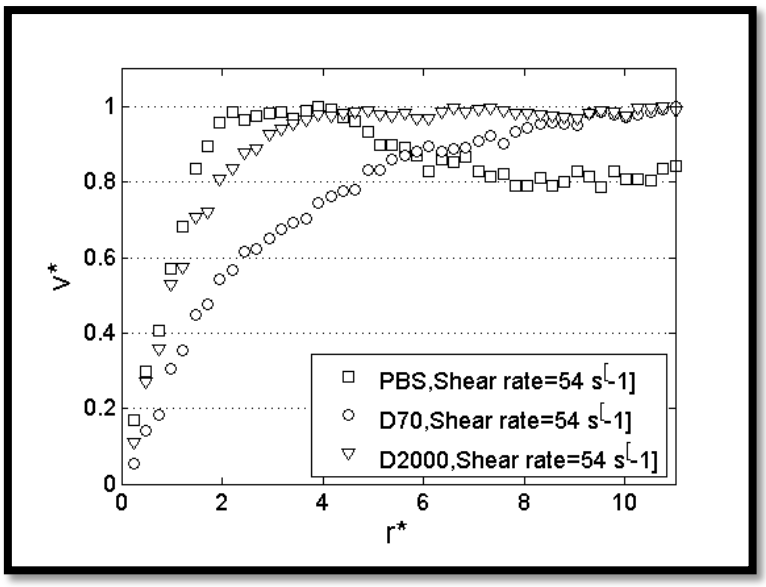

Figure 30.Velocity profiles for PBS WALL, D70, D2000 comparison graphs at 54 s^{-1} shear rate

No trend is observed between the cases from r*=1 until r*=6. At r*=6 there is trend between the cases; for aggregating cases(D70 and D2000) the behavior is similar . PBS reaches its maximum velocity(near the wall) at $r^* = 2$ and for D70 and D2000 at $r^* = 11$. Another observation is that the behavior of D2000 is smoother than the other cases. PBS behaves differently; has lower V^* than the cases D70 and D2000.

3.1.9 Absolute mean velocity as function of the nominal shear rate

In this section, PIV data were scaled to absolute velocity values using a correction factor according to the frame rate and pixel resolution for each nominal shear case. The velocity data were converted to μm/s. The converted values of mean velocity and STD are presented in the following table for the following cases, PBS, D70, D2000 and at the different shear rates, for r*~8-11.

Table 2-Absolute mean velocity as function of the nominal shear rate

PBS WALL	MEAN VELOCITY (µm/s)	STD	D70	MEAN VELOCITY (µm/s)	STD	D2000	MEAN VELOCITY (µm/s)	STD
PBS WALL $2.5s^{-1}$	20	16	D70 $1s^{-1}$	35	90	D2000 $5s^{-1}$	35	11
PBS WALL $33s^{-1}$	250	300	D70 $5s^{-1}$	100	22	D2000 $11s^{-1}$	225	55
PBS WALL $54s^{-1}$	320	230	D70 $11s^{-1}$	225	35	D2000 $25s^{-1}$	550	150
			D70 $25s^{-1}$	450	160	D2000 $54s^{-1}$	1100	300
			D70 $54s^{-1}$	800	525			

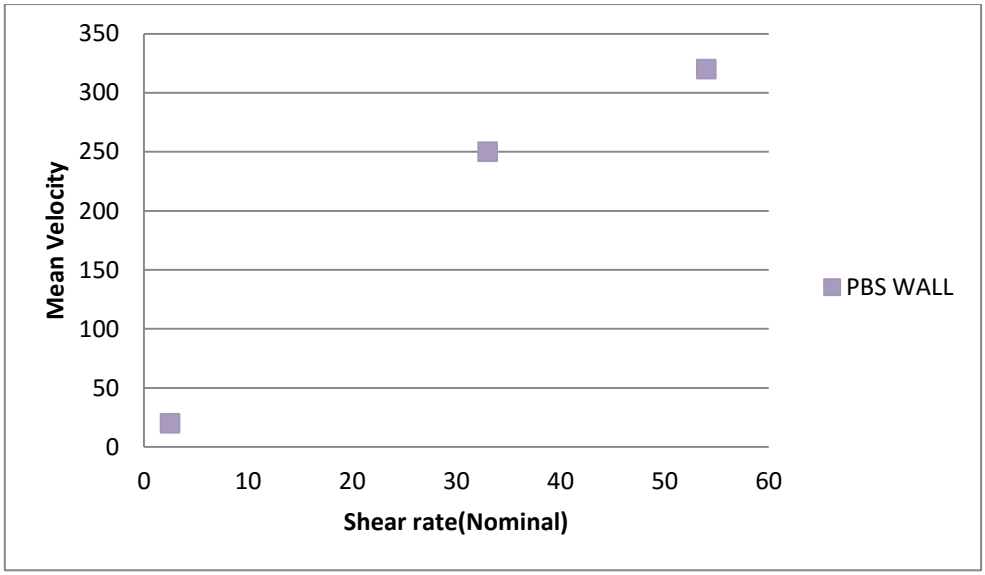

Figure 31. The Mean velocity values against nominal shear rate for the PBS case

In Figure 31 is presented the mean velocity of RBCs in the flow configuration for the PBS case and for the nominal shear rates of $2.5s^{-1}$, $33s^{-1}$ and $54s^{-1}$. We would expect to get zero velocities at the zero nominal shear as there will be no flow induced. The graph shows that increasing the shear rate the mean velocity is increased

proportionally.

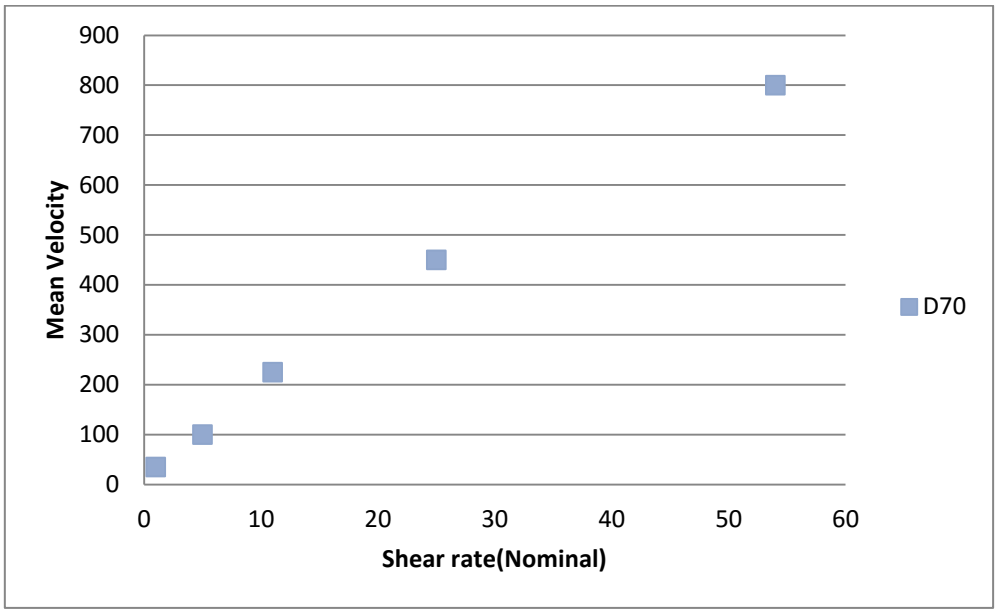

Figure 32. The velocity profile against radius gap of D70 at different shear rates

Figure 32 shows the velocity behavior of D70 velocity against nominal shear rate which is similar to the PBS case: The velocity is proportional to the nominal shear rate as expected.

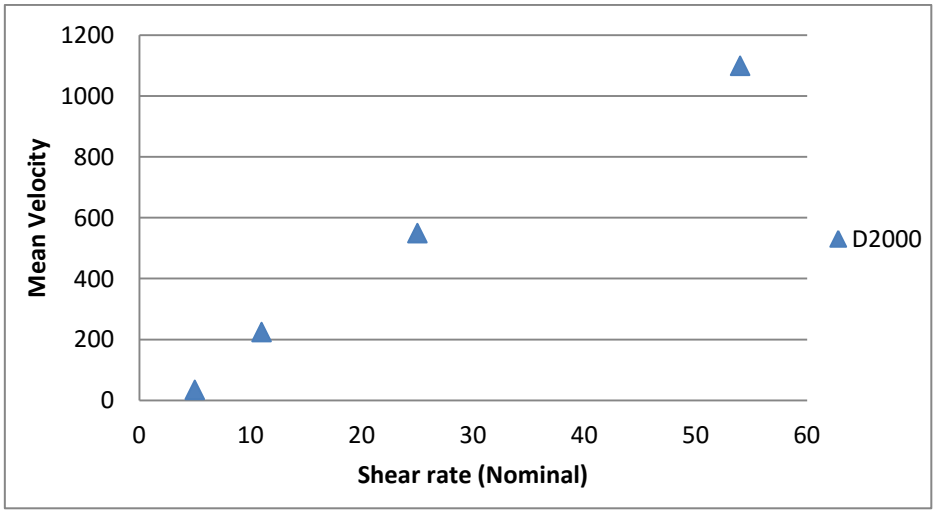

Figure 33. The velocity profile against radius gap of D2000 at different shear rates

In figure 33 is presented the velocity behavior of D2000 under different nominal

shear rates: again the proportionality of the velocity to the nominal shear rate is observed as expected.

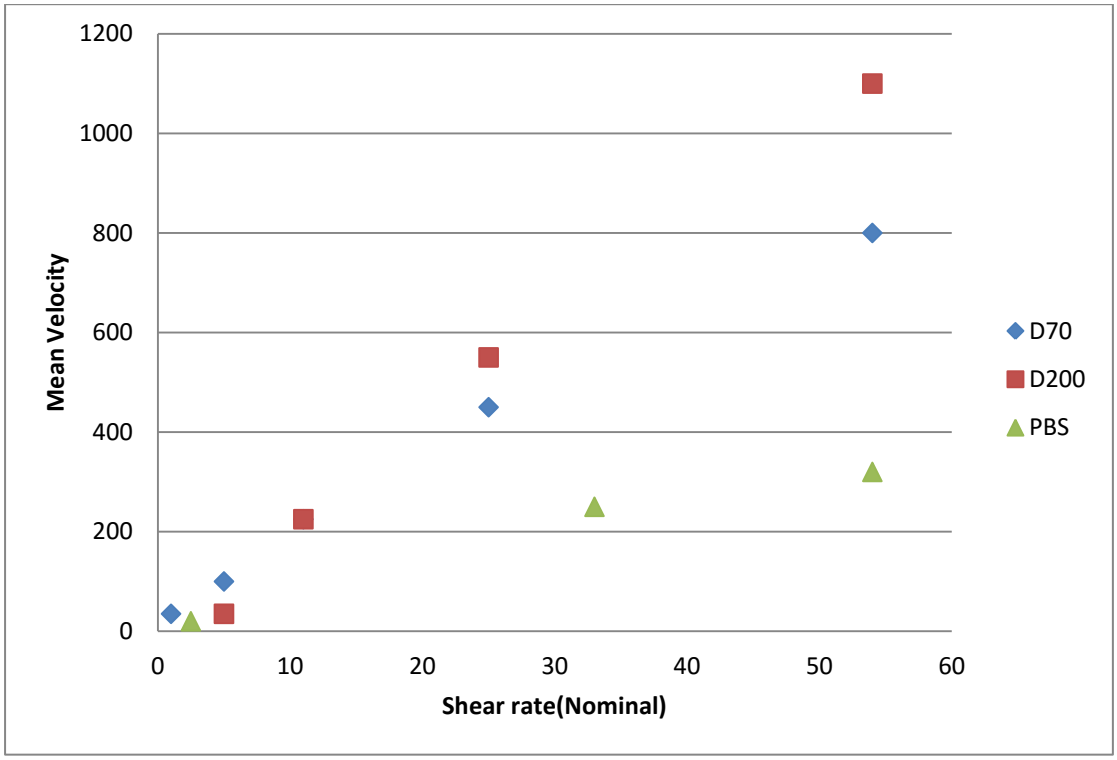

Figure34. The velocity profile against shear rate of PBS,D70 and D2000

Figure 34 shows the mean velocity behavior of RBCs in comparison for the cases of PBS, D70 and D2000, against shear rate. The velocity for the PBS case is lower than the cases of D70 and D2000, due to PBS is non aggregative case and the velocity cells follow the velocity of a plate (ESR). Another observation is that D70 and D2000 behave similarly ; at high shear rate is observed high value of velocity. Near the wall the velocity is approximately 0 due to wall slip condition; zero velocity at the wall.

3.2 Local shear rates measurements

One characteristic of the flow which is of particular interest is the local shear rate which develops due the existence of the extra boundary (the side wall) in the geometry. This boundary causes an additional plane of shear to develop and therefore the actual shear conditions in flow cannot be accurately represented by the nominal shear rate. It would therefore by appropriate to find the region at which the local shear is dominant over the nominal shear.

3.2.1 Calculation of the local shear for the PBS case

In this section we will calculate the local shear rate of the cases PBS, D70 and D2000 and we will examine the effect of radius and gap under different local shear rates. The difference between local shear rate and the nominal shear rate (global) is that in local shear rate the wall effect is taken into account. The nominal shear rate represents a global shear rate. Local shear rate will be more appropriate closer to boundaries, i.e. near the wall.

The effect will be analyzed and presented in graphs of normalized shear rate $\gamma^* = \gamma local\dot{}/\gamma nomınal$, against normalized radius (r^*) . Formula 21 describes briefly the following figures.

$$\gamma l\acute{o}cal = \frac{\dot{du}}{dr*} = \frac{\Delta u}{\Delta r*} \quad (21)$$

In figure 35 is presented the local shear rates measurements of PBS case. The graphs are presented as a normalized shear rate against normalized radius.

Specifically at shear rate $2.5s^{-1}$ in figure 35(a) the highest $\dot{\gamma}^*$ on is observed at $r^* = 1$. This means that the cells experience the highest local shear rate value near the wall at a distance of one channel height from the wall. The shear rate is decreased significantly at $r^* \sim 3.5$.

In figure 35(b) is presented the local shear rate of $33s^{-1}$. The highest $\dot{\gamma}^*$ is at $r^* = 1$. As in the previous shear rate of $2.5s^{-1}$ is observed similar behavior; the cells reaches the highest local shear rate value near the wall and the shear diminishes at $r^* \sim 2$.

Figure 35 (c) shows the effect of gap at shear rate $54s^{-1}$. The maximum local shear rate is recorded near the wall at $r^* = 1$. At $r^* = 3$ the local shear has been decreased to minimum value.

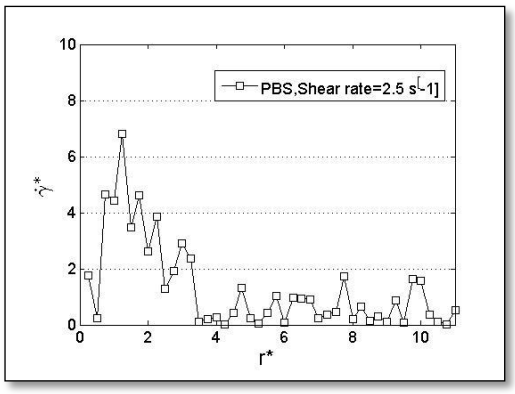

(a)

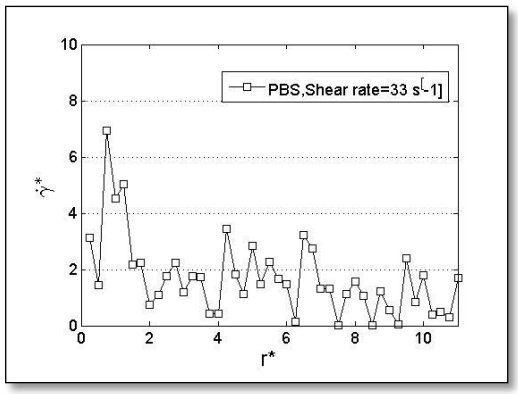

(b)

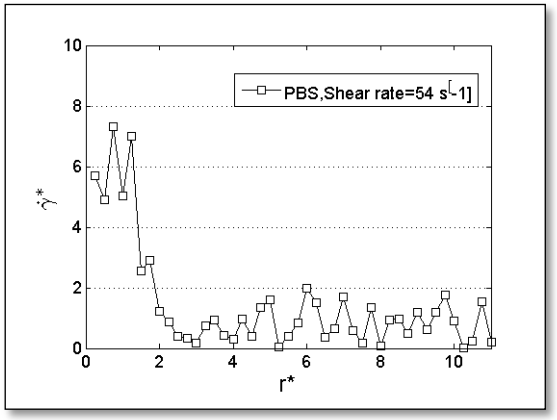

(c)

Figure 35. PBS WALL gradient graphs a) PBS WALL gradient graphs, shear rate 2.5s^{-1} b) PBS WALL gradient graphs, shear rate 33s^{-} c) PBS WALL gradient graphs, shear rate 54s^{-1}

3.2.2 Calculation of the local shear for the D70 case

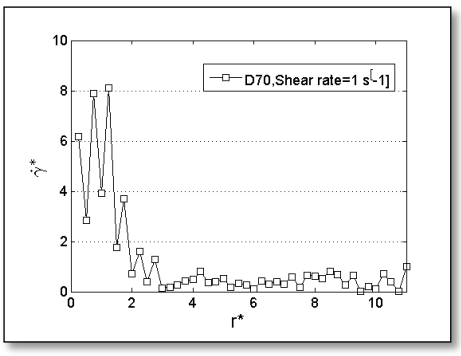

(a)

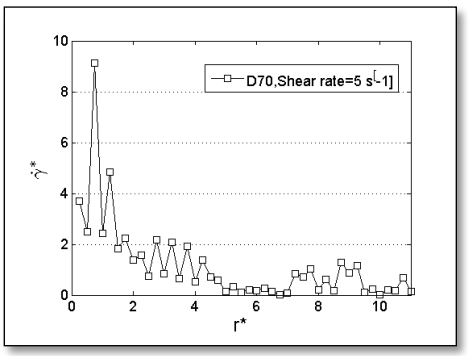

(b)

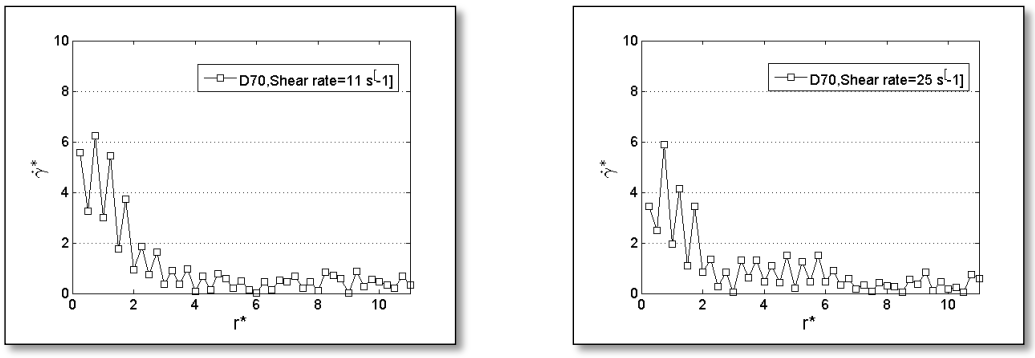

(c) **(d)**

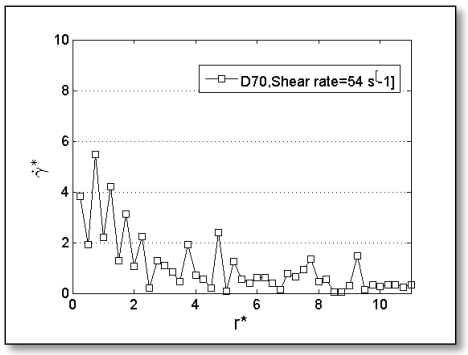

(e)

Figure 36. D70 gradient graphs a) D70 gradient graphs, shear rate $1s^{-1}$ b) D70 gradient graphs, shear rate $5s^{-1}$ c) D70 gradient graphs, shear rate $11s^{-1}$ d) D70 gradient graphs, shear rate $25s^{-1}$

In figure 36 is presented the local shear rates measurements of the cases D70, $1s^{-1}$, $5s^{-1}$, $11s^{-1}$, $25s^{-1}$, $54s^{-1}$. At the shear rate of $1s^{-1}$ in figure 36(a) the highest $\dot{\gamma}^*$ on the gap is at $r^* = 1$, the shear rate is increased significantly at $r^* = 3$. For the $5s^{-1}$ case in figure 36(b)is observed similar behavior; the highest $\dot{\gamma}^*$ on the gap is again at $r^* = 1$. and at $r^* \sim 5$ we observe the minimum local shear. For the shear rate of $11s^{-1}$ (Figure 36(c)) the maximum local shear rate is observed near the wall at $r^* \sim 1$. Graph gets smoother away from the wall, specifically at $r^* = 4$. A similar behavior is observed at the shear rate of $25s^{-1}$ in figure 36(d) and $54s^{-1}$ in figure 36(e).

3.2.3 Calculation of the local shear for the D2000 case

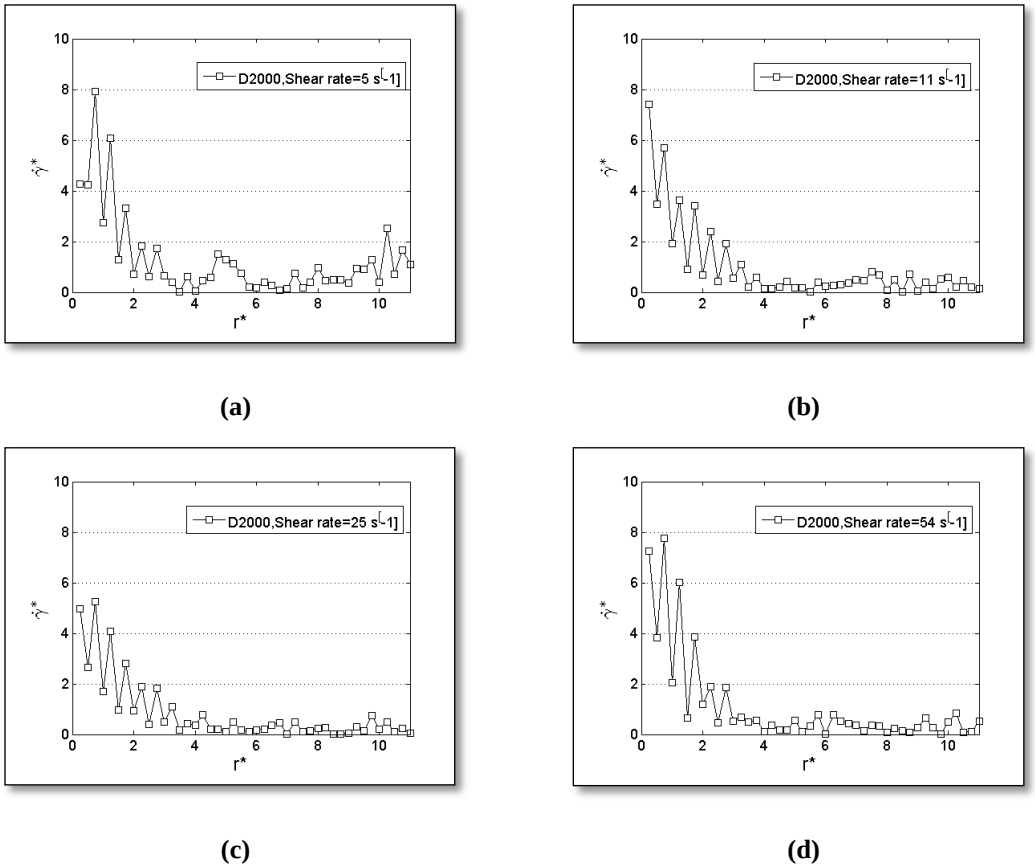

Figure 37. D2000 gradient graphs a) D2000 gradient graphs, shear rate $5s^{-1}$ b) D2000 gradient graphs, shear rate $11s^{-1}$ c) D2000 gradient graphs, shear rate $25s^{-1}$ d) D2000 gradient graphs, shear rate 54

In figure 37 is presented the local shear measurements for the D2000 case. In general the behavior is similar in all cases: for the nominal shear rate of $5s^{-1}$ is observed that the highest $\dot{\gamma}^*$ on is observed at $r^* = 1$ and the local shear minimizes at around $r^* = 3.75$ is presented the local shear rate of. The highest $\dot{\gamma}^*$ for the $11s^{-1}$ case in figure 37(b) is at $r^* = 0.1$ and for the $25s^{-1}$ is at $r^* = 0.5$ with minimum at $r^* = 4$. Figure 37(d) shows the effect of gap at shear rate $54s^{-1}$ with maximum local shear rate at $r^* = 0.75$ and minimum at $r^* = 4$.

3.3 Aggregation indices

In this section an attempt to characterize the RBC aggregation phenomenon will be presented. In the present work STD values of Mean Velocity, STD and coefficient of variation of the grayscale intensity values in the images are presented and analyzed as possible indices of aggregation. Blood images were analyzed using JPIV and matlab algorithms. Velocity fields were calculated and mean velocity was produced in microns/s. Blood samples of PBS, D70 and D2000 were processed , giving by

equation (20) the coefficient of variation. The STD indicates the amount of dispersion of velocity or intensity values about their mean values. A standard deviation close to 0 indicates that the data points tend to be very close to the highest standard deviation. A standard deviation close to 60% of the distribution of the data, indicates that the data points are ~1STD away from the mean values.

3.3.1. STD of velocity as an index of aggregation

STD was processed in combination with velocity values. Velocity values of samples were calculated with matlab algorithm providing the mean velocity value. The calculation of deviation was calculated from the subtraction square root of velocity value and mean velocity. The following formula describes the behavior of CV, according to STD and Mean velocity:

$$CV = \frac{STD}{Mean\ Velocity} \qquad (20)$$

CV=Coefficient of variation

STD=Standard deviation

The variance is the mean of subtraction square root of velocity value and mean velocity and the population standard deviation is equal to the square root of the variance. The values of standard deviation for each case were recorded at r* =11 and presented in Table 3 bellow:

Table 3-STD of velocity as an index aggregation

PBS WALL	**STD**	D70	**STD**	D2000	**STD**
PBS WALL 2.5s^{-1}	0.4597	**D70 1s^{-1}**	2.6448	**D2000 5s^{-1}**	1.1215
PBS WALL 33s^{-1}	2.2334	**D70 5s^{-1}**	0.6170	**D2000 11s^{-1}**	0.8094
PBS WALL 54s^{-1}	1.7557	**D70 11s^{-1}**	1.0812	**D2000 25s^{-1}**	2.1454
		D70 25s^{-1}	2.1361	**D2000 54s^{-1}**	3.8267
		D70 54s^{-1}	4.1032		

A first observation from the values in the above table is that the STD values in the PBS case are lower than the other two cases. This is more apparent where the STD values are plotted versus the nominal shear rates in Figures 39(a), (b) and (c), for the PBS, D70 and D2000 respectively.

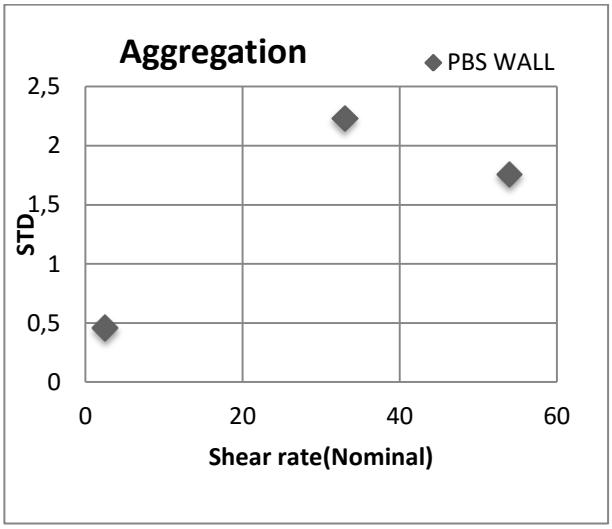

(a)

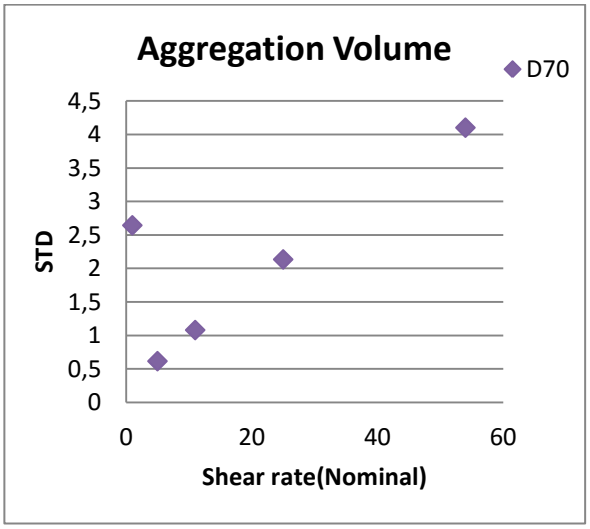

(b)

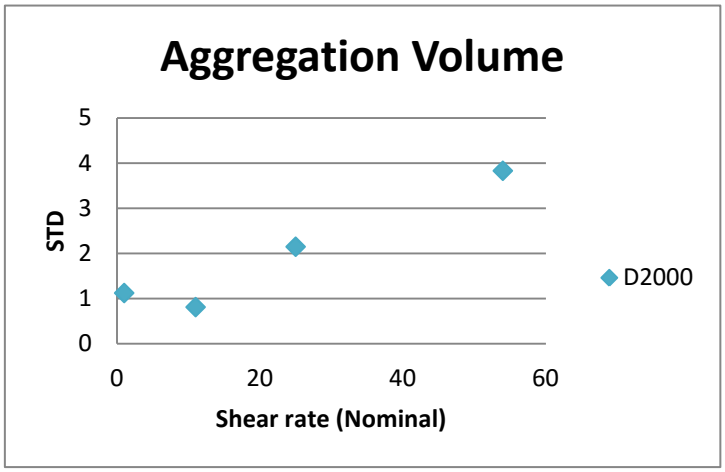

(c)

Figure 38. The aggregation volume of PBS, D70 and D2000

In Figure 38 (a) is presented the STD for the PBS case and for the shear rates of $2.5s^{-1}$, $33s^{-1}$ and $54s^{-1}$. Shear rate $33s^{-1}$ and $54s^{-1}$ have similar values; the data tend to spread in contrast with shear rate $2.5s^{-1}$ which has smaller dispersion. The frame rate which was used for PBS it was 100 for $2.5s^{-1}$, and 400 for the cases of $33s^{-1}$ and $54s^{-1}$ which that as greater is the FR as greater is the dispersion

Figure 38(b) shows the STD of velocity data for the D70 case. In the specific graph the magnitude of STD for the higher shear rate of $54s^{-1}$ is the maximum. This indicates that the data at low shear rates tend to be closer to the mean value so there is small dispersion. The frame rate which was used for D70 it was 100 for $1s^{-1}$, $5s^{-1}$, $11s^{-1}$, 200 for $25s^{-1}$and 400 for the case of $54s^{-1}$ which that as greater is the FR as greater is the dispersion.

In figure 38(c) is presented the standard deviation graph against r* of D2000 at different nominal shear rates $5s^{-1}$, $11s^{-1}$, $25s^{-1}$ and $54s^{-1}$.In the specific graph the magnitude of STD for the lower shear rate of $5s^{-1}$ and $11s^{-1}$ is the minimum. This indicates that the dispersion of the data at low shear rates is smaller compared to the higher shear rates. As the STD increases, the data tends to spread more. Above $5s^{-1,}$ there is a trend: as we increase the shear rate the dispersion increases. The frame rate which was used for D2000 it was 30 for $5s^{-1}$, 200 for the case of $11s^{-1}$ and $25s^{-1}$ and 400 for $54s^{-1}$ which that as greater is the FR as greater is the dispersion.

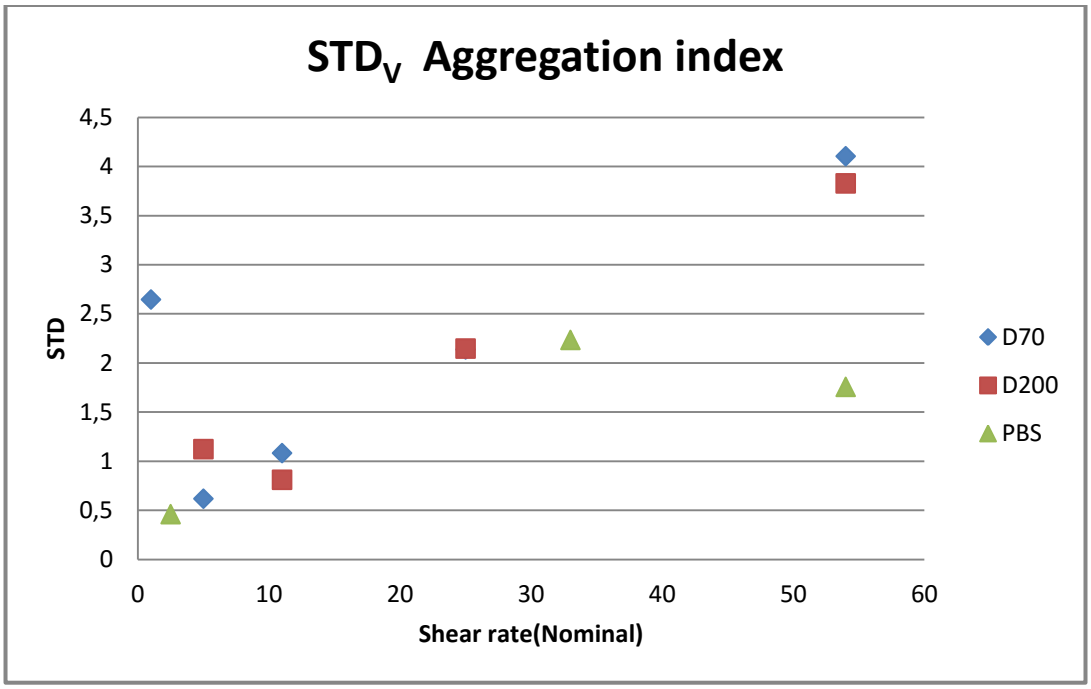

Figure 39.STDv Aggregation index for PBS,D70 and D2000

The standard deviation of velocity against the nominal shear rate for all cases (PBS,D70 and D2000) is presented in comparison in Figure 39. The behavior of STD for the PBS is different from the behavior of Dextrans. STD in D70 and D2000 behaves similarly; small dispersion is observed in low shear rate, ex. at $2.5s^{-1}$ increasing for the higher shear rates. For the aggregative cases,D70 and D2000 we observe large aggregates. Increasing even more the shear rate we will observe that the aggregates breaks down due to the shear forces, however aggregates persist even at higher shear rates (see Figure 39) .

STD is a potential index of aggregation when is compared with the dispersion and aggregation of cells. The data at low shear rates tend to be closer to the mean value so there is small dispersion. In the other hand at high shear rates the data is away from the mean value causing aggregation . The curve of the slop for the case of D70 seems to be linear; this means that D70 can be the intermediate level of PBS(non-aggregating case) and D2000(aggregating case). Another observation is the decreasing of STD value for the case of PBS at $54s^{-1}$. This indicates that away from the wall the cells follow the velocity of the plate, due to ESR.

3.3.2 Coefficient of variation of image intensity

In this part of the work the coefficient of variation (CV) in the image intensity data is presented and analyzed. Matlab software used for the development of the algorithms which performed the intensity calculations in the images of PBS, D70 and D2000. Table 4 shows the results of processing. The table shows that there are small differences between the CV values in the different cases. CV can be considered as an aggregation index, measuring the standardized relative STD. It can be calculated as the percentage of a ratio of mean STD against mean Intensity.

Table 4-Coefficient of variation of image intensity

PBS			
Shear rate	**Mean Intensity**	**Mean STD**	**CV**
2.5s^{-1}	65.31	12.14	0.1860
33s^{-1}	67.56	14.60	0.2162
54s^{-1}	59.91	13.08	0.2185
D70			
2.5s^{-1}	91.93	19.47	0.2118
33s^{-1}	87.37	17.42	0.1994
54s^{-1}	89.12	18.22	0.2044
33s^{-1}	95.31	19.33	0.2028
54s^{-1}	88.60	19.22	0.2169
D2000			
33s^{-1}	97.58	23.81	0.2441
54s^{-1}	93.46	21.18	0.2267
33s^{-1}	90.84	20.32	0.2237
54s^{-1}	90.42	21.23	0.2248

CHAPTER 4. DISCUSSION

4.1 General observations on the velocity behavior

In figure 17, the behavior of PBS velocity at shear rates $2.5s^{-1}$, and $33s^{-1}$ is found to be similar: close to the wall were observed small velocities increasing as r^* increases and reaching a maximum at around $r^* = 11$. On the other hand the behavior of $54s^{-1}$ close to wall is different, possibly due to lower sedimentation occurring in the flow; at high shear rates the cells are better distributed in the flow and they do not sediment easily. There are no trends observed between different shear rates close and away from the wall, where the velocity profile becomes more smooth for all the shear rates.

The PBS cases can be considered closer to the Newtonian case as the aggregation effects are not apparent in the flow. For this reason the analytical solution has been produced and shown in Figure 23. In Figure 23 the expected behavior of velocity is illustrated. The most significant difference between the theoretical solution and the experimental data for the PBS case is that the curve of the slop for the case of D70 seems to be linear; this means that D70 can be the intermediate level of PBS(non-aggregating case) and D2000(aggregating case).

The experimental solution was produced from the velocity analysis of RBCs. In figure 17, for the case of PBS is presented the velocity behavior of RBCs at 2.5, 33 and 54 s^{-1}. The curve of the slop changes significantly for different shear rates; this means that each shear rate behaves differently. The experimental solution can be present the velocity behavior of RBCs qualitatively.

The theoretical solution was produced from the analytical solution of Laplace equation which represents the heat transfer along rectangular plate. The solution was given in equation (13) and the velocity profiles for the PBS case was presented in figure 23. The main observation for theoretical solution is the slop; no curves are observed in contrast with experimental solution. The theoretical solution can be present the velocity behavior of RBCs quantitatively.

Another observation is the decreasing of STD value for the case of PBS at $54s^{-1}$. This indicates that away from the wall the cells follow the velocity of the plate, due to ESR. In addition figure 16 shows representative images for non-aggregating (PBS)

and aggregating cases(D70 and D2000). In case of PBS, at low shear rate and high shear rate changes in structure are not presented as the PBS is not aggregating case .

The velocity profiles from all shear rates tested in the D70 case are presented in comparison in Figure 25. An interesting pattern is observed in Figure 25; very similar behavior for r* between 0.1 and around 2 and between approximately 7 and 11. More interestingly a trend is observed for the velocities between r*= 1 and 7; the velocities in the smaller shear rates (e.g. in 1, 5 and 11) seem to develop faster than those in the higher shear rates (25 and 54 s^{-1}). This could be attributed to fact that at lower shear rates the cells sediment faster and a greater population of cells gain higher velocities from the rotating plate. Note that the maximum velocity occurs at the rotating plate.

Velocity profiles for all the D2000 cases are plotted in comparison in Figure 27. The behavior of the velocities in all shear rates is similar: close to the wall were observed small velocities increasing as r^* increases and reaching a maximum at $r^* = 4$. Here the trend observed in Figure 25 (the D70 case) is not present.

Shear rate 5 s^{-1}

In figure 28 is presented the velocity behavior of comparison cases PBS ,D70 and D2000 for shear rate 5s^{-1}. At the case of PBS, the first three points, following different pattern from the other points; velocity fluctuation possibly occurring in the flow due to ESR .At high shear rates the cells are better distributed in the flow and they do not sediment easily. There are no trends observed between different shear rates close and away from the wall, where the velocity profile becomes more smooth for all the shear rates. In addition near the wall (until $r^* = 1$) all the cases seems to behave similarly. At the end of geometry D2000 behaves differently; has lower V^* than the cases D70 and PBS. D70 and PBS reaches them maximum at $r^* = 11$.

Shear rate 25 s^{-1}

Similarly to the previous cases the behavior of velocity presented in figure 29 as normalized velocity(V^*) against normalized radius(r^*). Effects of the unevenness at the vertical wall due to the adhesive of the silicon sheet seem minimized in the present cases. Zero velocities would be expected at the wall, however due to the slip effect at the wall no zero velocities where observed. Another observation is that away from the wall the velocity profile becomes more smooth and flat. Another observation

is that away from the wall at $r^* = 6$, D70 and D2000 behaves similarly and reaches them maximum velocity at $r^* = 11$.

Shear rate 54 s^{-1}

In figure 30 is presented the velocity behavior of PBS ,D70 and D2000 for shear rate 54s^{-1}. An interesting pattern between the case D70 and D2000 is observed at r*=11; the velocity reaches at its maximum. The velocity of PBS at r*=11 is significantly lower that Dextrans as it was expected. A trend is observed for all cases at r*=6 until r*=11; as increasing shear rate as the velocity does.

Shear rate 5,25,54 s^{-1}

The effect of aggregation affect the mean flow conditions and this can be explained in comparison graphs of 5,25 and 54s^{-1}. In figure 28 is observed that at the end of geometry D2000 behaves differently; has lower V^* than the cases D70 and PBS ; this means that the effect of aggregation effect the flow conditions. Similarly in figure 29 and 30 is observed that the effect of aggregation effect the flow condition; high value of V^* in case of D2000 and D70 is presented.

4.2 General observations on the local shear characteristics

One characteristic of the flow which develops due the existence of the extra boundary (the side wall) in the geometry is very interesting. This boundary causes an additional plane of shear to develop and therefore the actual shear conditions in the flow cannot be accurately represented by the nominal shear rate. General observations on the local shear characteristics prove that aggregation has an effect on it. Specifically for the cases of PBS the highest $\dot{\gamma}^*$ on is observed at $r^* = 1$. This indicates that the cells reach the highest local shear rate value near the wall at a distance of one channel height from the wall. The local shear is minimized around $r^* \sim 3$.

D70 and D2000, aggregative cases behaves similarly as it was expected. The highest $\dot{\gamma}^*$ on the gap is observed at $r^* = 1$, and the shear rate is minimized significantly at $r^* \sim 4$.

A significant difference is observed on non-aggregating(PBS) case and aggregative cases(D70 and D2000); The local shear for PBS is minimized around $r^{*}\sim 3$ and for aggregating cases at $r^{*}\sim 4$.

4.3 Aggregation indices

The aggregation indices where developed for measuring the intensity of aggregation was based on velocity intensity, STD values of mean velocity, coefficient of variation in the image intensity and local shear measurements. Minimum aggregation is achieved when STD value is minimum, therefore at low CV values. A high CV value would indicate increased aggregation. Image processing with matlab algorithms was used for CV calculation and characterization of the aggregation. The aggregation indices could be used in the way of characterization of the phenomenon. In my opinion the best aggregation measurements which can characterize the phenomenon is the local shear measurements because this methodology takes in consideration the extra wall boundary which affects the behavior or RBCs.

4.4 Error analysis

The error analysis was based on the frame rate which was used for the cases. Frame rate, also known as frame frequency, is the frequency(rate) at which an imaging device displays consecutive images called frames. Frame rate is expressed in frames per second. The technique was facing a problem because for lower shear rates was used smaller frame rates. Higher Frame rates produces more accurate results.

CONCLUSIONS

The main outcome of this present work is that the flow of blood at low shearing flow conditions is dominated by the effects of RBC aggregation and other secondary effects. Analyzing the changes in the velocity profiles caused by the phenomenon of RBC aggregation and cell sedimentation can be support that the aggregation affects blood flow; in aggregative case of D70 and D2000 is observed medium for D70 and high aggregation for D2000 at low shear rates. This observation can be support in figure 29 as the D70 and D2000 behaves similarly; both cases reach its maximum at r*=11. Generally in figure 29 is observed that D70 and D2000 near the wall and away from the wall behave similarly in contrast with PBS. In the other case , PBS behaves differently; has lower V^* than the cases D70 and D2000, at r*=11. Similarly in figure 30 is observed similar behavior for D70 and D2000 at r*=11.

The effect of aggregation affect the mean flow conditions ; high value of V^* in case of D2000 and D70 is presented in figures 28,29 and 30 of comparison shear rates.

As the shear rate is increasing the aggregates broke down as individual cells as can be supported from the image intensity indices.PBS is non-aggregative case and no rouleaux formation is occurred.

The value of this work for other scientific fields is important since the results which provided would be useful in study of another simple or complex geometry and in another flow conditions. The present results could be the foundation for the determination useful tools in the field of Biomedical Engineering and generally in the field of medicine.

Bibliography

[1] Meiselman HJ. Red blood cell role in RBC aggregation:1963-1993 and beyond. Clin Hemorheol 1993;13:575-592

[2] Oguz K.Baskurt, M.D.,Ph.D., Blood Rheology and Hemodynamics and Herbert J.Meiselman,Sc.D

[3a] Oguz K.Baskurt,Department of Physiology, Faculty of Medicine, Akdeniz University,Antalya-Turkey.Pathophysiological Significance of Blood Rheology,September 16,2003

[3] Jonathan Dusting, Efstathios Kaliviotis, Stavroula Balabani, Michael Yianneskis,.2009.Coupled human erythrocyte velocity field and aggregation measurements at plysiological haematocrit levels.Journal of Biomechanics 42(2009) 1438-1443

[4]Baskurt OK, Meiselman HJ. Blood Rheology and Hemodynamics2003;p;436

[5] J.G.G Ledingham and David A. Warrell , Concise Oxford Textbook of Medicine,ISBN 0 19 262870 4

[6] Laura Dean. Blood Groups and Red Cell Antigens, Jump up to: Pierigè F, Serafini S, Rossi L, Magnani M (January 2008). "Cell-based drug delivery". Advanced Drug Delivery Reviews 60 (2): 286–95. doi:10.1016/j.addr.2007.08.029. PMID 17997501

[7] Laura Dean. Blood Groups and Red Cell Antigens, Jump up to: Pierigè F, Serafini S, Rossi L, Magnani M (January 2008). "Cell-based drug delivery". Advanced Drug Delivery Reviews 60 (2): 286–95. doi:10.1016/j.addr.2007.08.029. PMID 17997501

[8]Holsworth RE, Cho YI. “Hyperviscosity Syndrome: A Nutritionally-Modifiable Cardiovascular Risk Factor.” Advancing Medicine with Food and Nutrients, Second Edition. Ed. Ingrid Kohlstadt. Boca Raton: CRC Press. 2012

[9] Oguz K.Baskurt,Department of Physiology, Faculty of Medicine, Akdeniz University,Antalya-Turkey.Pathophysiological Significance of Blood Rheology,September 16,2003

[10] G. D. O. Lowe, J. C. Barbenel, C. D. Forbes Clinical Aspects of Blood Viscosity and Cell Deformability

[11] Schneider DJ, Taatjes DJ, Howard DB, Sobel BE. Increased reactivity of platelets induced by fibrinogen independent of its binding to the IIb-IIIa surface glycoprotein: a potential contributor to cardiovascular risk. *J Am Coll Cardiol* 1999; 33:261–6

[12] William F.Ganong, Review of Medical Physiololgy, fifteenth edition ,ISBN 0-8385-8438-1

[13] Oguz K.Baskurt,Department of Physiology, Faculty of Medicine, Akdeniz University,Antalya-Turkey.Pathophysiological Significance of Blood Rheology,September 16,2003

[14] Thomas B. 2001. Manual of Dietetic practice. The British Dietetic Association. Pp 505-535.

[15] e.g. G. W. Scott Blair *et al., J. Phys. Chem*., (1939) 43 (7) 853–864. Also the *de Waele-Ostwald* law, e.g Markus Reiner *et al., Kolloid Zeitschrift*(1933) 65 (1) 44-62

[16] Fundamentals of Materials Science and Engineering, William D. Callister, John Wiley and Sons, 2nd International edition (September 3, 2004)

[17] Introduction to Fluid Mechanics , notes.

[18] e.g. G. W. Scott Blair *et al., J. Phys. Chem*., (1939) 43 (7) 853–864. Also the *de Waele-Ostwald* law, e.g Markus Reiner *et al., Kolloid Zeitschrift*(1933) 65 (1) 44-62

[19] M.E. Charles and L.U. Lilleleht, J. Fluid Mech., 22 (1965) 217

[20]Analysis of the Casson and Carreau-Yasuda non-Newtonian blood models in steady and oscillatory flows using the lattice Boltzmann method

[21,22,23]Jump up^ *Kirby, B.J. (2010).* Micro- and Nanoscale Fluid Mechanics: Transport in Microfluidic Devices. *Cambridge University Press.*ISBN 978-0-521-11903-0.

[24] Nnguyen and Wereley. Fundamentals of Microfluidics.

[25]Jump up^ Kirby, B.J. (2010). Micro- and Nanoscale Fluid Mechanics: Transport in Microfluidic Devices. Cambridge University Press.ISBN 978-0-521-11903-0

[26] Rampling M. W., Plasma- Protein Induced Aggregation of Erythrocytes: Its causes, Estimation and Effects of Blood Flow, Studia Biophys.,134, 91-94,1989.

[27]S.O.Sowemimo,Coker,P.Whittingstall,L.Pietsch,R.M.Bauersachs,R.B.WenbyandH.J.Meiselman,Effectsofcellular factors on the aggregation behaviour of human, rat and bovine erythrocytes, Clin. Hemorheol. 9 (1989), 723–737.

[28] H. Schmid-Schönbein, E. Volger and H.J. Klose, Microrheology and light transmission of blood, Pflügers Arch. 333 (1972), 140–155.

[29] Rampling M. W. and Whittingstall P., A Comparison of five methods for estimating red cell aggregation, Klin. Wochensch., 64, 1084- 1088, 1986

[30] Hitt D. L. and Lowe M. L., Spatial Analysis of Red Blood Cell Aggregation for in vitro tube flow, Proc. World Cong. on Microcirc., Messmer, K and Kubler, W. M., (Eds.), Monduzzi Editore, Bologna, Italy, 207- 211, 1996.